A Novel Progressive Gaussian Approximate Filter for Tightly Coupled GNSS/INS Integration

Mingming Bai, Yulong Huang, *Member, IEEE*, Yonggang Zhang, *Senior Member, IEEE*, and Guangle Jia

***Abstract*— In this article, we focus on addressing the nonlinear filtering problem with large prior uncertainty but high measurement accuracy, which may be encountered in the application of tightly coupled global navigation satellite system (GNSS)/inertial navigation system (INS) integration. Although the existing methods, such as progressive Gaussian approximate filter (PGAF), can address this problem, it has poor estimation accuracy. To improve the estimation accuracy of PGAF, the step sizes as well as the measurement noise covariance matrix (MNCM) are jointly estimated based on the variational Bayesian approach, from which a novel PGAF with variable step size is developed. Tightly coupled GNSS/INS integration simulations illustrate that the proposed filter outperforms the existing methods both in estimation accuracy and rate of convergence.**

***Index Terms*— Gaussian approximation, nonlinear filtering, progressive filtering, variable step sizes.**

I. Introduction

INTEGRATING information from global navigation satellite system (GNSS) with that from inertial navigation system (INS) has been proven to be an efficient methodology of navigation due to its complementary error property [1]–[4]. The most common integration scheme for GNSS/INS is the loosely coupled approach, where the measurements are chosen as the position and velocity information provided by the GNSS receiver [5], [6]. A tightly coupled integration scheme can be employed to promote the performance, where the raw GNSS pseudorange and pseudorange rate information is utilized directly to assist the INS. Generally, tightly coupled integration systems outperform the loosely coupled integration systems because more nuisance and noise terms can be controlled and taken into consideration. Apart from that, another important advantage of the tightly coupled integration is that even fewer satellites are needed. The tightly coupled approach can enable the INS errors to be continually corrected even if the number of visible satellites is less than four [7]–[9], whereas for loosely coupled integration systems, at least four satellites are needed to determine the position and velocity of receiver. This increases the robustness of the tightly coupled integration systems against the satellite signal obstruction. However, nonlinear measurement models are formed because of the direct use of the raw pseudorange and pseudorange rate in tightly coupled integration systems. Although the extended Kalman filter (EKF) can be directly used to carry out the tightly coupled GNSS/INS integration by linearizing the nonlinear integration model based on the first-order Taylor expansion, it suffers from substantial approximation errors for the case of high nonlinearity. Therefore, a mass of nonlinear filters have been proposed.

Although it lacks closed-form solutions for the posterior probability density functions (PDFs) of a nonlinear state-space model, Gaussian approximate filters (GAFs), which approximate the joint PDFs of the state and measurement as well as the posterior PDFs as Gaussian PDFs, are the most common approaches having been widely applied. The GAFs balance the estimation performance and the computational complexity properly [10]–[15]. Based on different numerical techniques to calculate the Gaussian weighted integral, a batch of GAFs have been derived, such as unscented Kalman filter (UKF) [14], cubature Kalman filter (CKF) [15], high-degree CKF [16], embedded CKF [17], interpolatory CKF [18], and sparse-grid quadrature filter [19], stochastic integration filter [20]. Nevertheless, these standard GAFs mentioned earlier may perform poorly when the situation with large prior uncertainty but high measurement accuracy is encountered [21], [22]. In the loosely coupled integration, the employment of low-cost inertial sensors and violent maneuvering may lead to process uncertainty, which has been solved by some robust methods, such as Huber's M-estimation method in [23] and the student's t-based filter in [24]. However, in the tightly coupled GNSS/INS integration, the large prior uncertainty may be induced by some reasons, such as the employment of low-cost inertial sensors, the violent maneuvering of vehicles, and the inevitably accumulated linearization approximate errors. Besides, the high-accuracy pseudorange and pseudorange rate measurements are usually available when a large number of satellites are visible [25], [26]. The estimation accuracy of the standard GAFs may degrade dramatically in such situations of tightly coupled GNSS/INS integration. Another powerful method to handle the nonlinear and non-Gaussian problems is the particle filter (PF) [27]. Unfortunately, the PF has poor estimation accuracy in high-dimensional situations, such as the tightly coupled GNSS/INS integration [28]. Apart from that,

Manuscript received June 6, 2019; accepted July 19, 2019. Date of publication July 31, 2019; date of current version May 12, 2020. This work was supported in part by the National Natural Science Foundation of China under Grant 61773133 and in part by the Fundamental Research Funds for the Central Universities under Grant 3072019CFJ0411 and Grant 3072019CFT0401. The Associate Editor coordinating the review process was Daniel Belega. *(Corresponding author: Yulong Huang.)*

The authors are with the Department of Automation, Harbin Engineering University, Harbin 150001, China (e-mail: mingming.bai@hrbeu.edu.cn; heuedu@163.com; zhangyg@hrbeu.edu.cn; jiaguangle2017@163.com).

Color versions of one or more of the figures in this article are available online at http://ieeexplore.ieee.org.

Digital Object Identifier 10.1109/TIM.2019.2932155

the estimation accuracy of PF depends heavily on the number of samples, which results in a heavy computational burden. A better compromise between the estimation accuracy and the computational burden needs to be proposed.

Aiming at tackling the problem aforementioned, some iterated GAFs have been proposed. The iterated EKF (IEKF) [29] is an improved version of EKF, which linearizes the measurement function around the maximum a posterior (MAP) estimate and exhibits good estimation accuracy in some cases with low measurement noise, and the iterated posterior linearization filter (IPLF) [22] can be deemed as an iterated statistical linear regression (SLR) with respect to the posterior. However, both of them involve the measurement information at one time, which degrades their approximate performances. The progressive Gaussian filters (PGFs) are first proposed in [30] and [31] based on the strategy of discretizing the continuous PDFs by the Dirac mixture approximate method. The PGFs include the measurement information gradually, but the estimation accuracy of that depends heavily on the number of samples. An EKF with recursive measurement update is derived in [32], whereas it suffers from the substantial approximation errors. Under the Bayesian framework, a general scheme of progressive GAFs (PGAFs) has been proposed in [33], where the intermediate posterior PDFs as well as the intermediate joint PDFs are approximated as Gaussian and the measurement likelihood PDFs is included progressively, which result in better estimation accuracy. However, the performance of the existing PGAF depends heavily upon the selection of step sizes, and the estimation accuracy of PGAFs degrades dramatically when unreasonable step sizes are set. Furthermore, during the implementation of the existing PGAFs, significant integral approximation errors are generated and inevitable, which is the main source of linearization approximate errors and also degrades the estimation performance. We model this integral approximation errors as additional pseudo-measurement noise.

To improve the estimation performance of the existing PGAFs, in this article, a novel PGAF with variable step size (VS-PGAF) and adaptive measurement noise covariance matrix (MNCM) is developed, in which the state vector, the step sizes, as well as the inaccurate MNCM are jointly estimated based on the variational Bayesian (VB) method. The inaccurate MNCM is often caused by the moderately time-varying practical environment, the integral approximation errors, and other non-modeling errors. The posterior PDFs of the state vector, the inaccurate MNCM, as well as the step size are updated as Gaussian, inverse-gamma (IG), and truncated gamma distributions, respectively. The proposed filter is applied to an application for tightly coupled GNSS/INS integration, where, to reduce the linearization approximation errors, the nonlinear measurement models with respect to the pseudorange and pseudorange rate are built. Tightly coupled GNSS/INS integration simulations results illustrate that the proposed filter outperforms the existing filters not only in estimation accuracy but also in the rate of convergence under the situation with large prior uncertainty but high accuracy. The proposed filter also performs well in the regular situation.

The remainder of this article is arranged as follows. Section II presents the problem statement of the state-of-the-art PGAF. The VS-PGAF is developed in Section III. In Section IV, the proposed filter is applied to the tightly coupled GNSS/INS integration applications. Finally, conclusions are drawn in Section V.

II. Problem Statement

Consider the following nonlinear stochastic state-space model:

$$\begin{cases} \mathbf{x}_k = \mathbf{f}_{k-1}(\mathbf{x}_{k-1}) + \mathbf{w}_{k-1} \\ \mathbf{z}_k = \mathbf{h}_k(\mathbf{x}_k) + \mathbf{v}_k \end{cases} \tag{1}$$

where k is the discrete-time index. $\mathbf{x}_k \in \mathbb{R}^n$ and $\mathbf{z}_k \in \mathbb{R}^m$ are the state vector and the measurement vector, respectively. $\mathbf{w}_k \in \mathbb{R}^n$ and $\mathbf{v}_k \in \mathbb{R}^m$ are mutually independent Gaussian white noise vectors satisfying $\mathbf{w}_k \sim \mathrm{N}(\mathbf{w}_k; \mathbf{0}, \mathbf{Q}_k)$ and $\mathbf{v}_k \sim \mathrm{N}(\mathbf{v}_k; \mathbf{0}, \mathbf{R}_k)$, respectively. The initial state vector $\mathbf{x}_0$ satisfies $\mathbf{x}_0 \sim \mathrm{N}(\mathbf{x}_0; \hat{\mathbf{x}}_{0|0}, \mathbf{P}_{0|0})$, which is independent of $\mathbf{w}_k$ and $\mathbf{v}_k$, where $\mathrm{N}(\cdot; \nu, \mathbf{V})$ presents the Gaussian distribution with mean ν and covariance matrix $\mathbf{V}$.

Nonlinear filtering is designed to estimate unknown system state $\mathbf{x}_k$ based on noise contaminated measurements $\mathbf{z}_{1:k}$, where $\mathbf{z}_{1:k} = \{\mathbf{z}_j\}_{j=1}^k$ denotes the measurements from time index 1 to time index k. For this purpose, it is necessary to obtain the posterior PDF of system state $\mathbf{x}_k$ [15], which, normally, can be obtained by two steps: time update and measurement update. In the time update phase, the one-step predictive PDF $p(\mathbf{x}_k|\mathbf{z}_{1:k-1})$ of system state is calculated as follows:

$$p(\mathbf{x}_k|\mathbf{z}_{1:k-1}) = \int p(\mathbf{x}_k|\mathbf{x}_{k-1}) p(\mathbf{x}_{k-1}|\mathbf{z}_{1:k-1}) d\mathbf{x}_{k-1} \tag{2}$$

where $p(\mathbf{x}_{k-1}|\mathbf{z}_{1:k-1})$ denotes the posterior PDF at last time index $k-1$, and $p(\mathbf{x}_k|\mathbf{x}_{k-1})$ denotes the state transition PDF.

In the measurement update phase, the posterior PDF $p(\mathbf{x}_k|\mathbf{z}_{1:k})$ of system state is calculated as follows:

$$p(\mathbf{x}_k|\mathbf{z}_{1:k}) = \frac{p(\mathbf{x}_k, \mathbf{z}_k|\mathbf{z}_{1:k-1})}{p(\mathbf{z}_k|\mathbf{z}_{1:k-1})} \tag{3}$$

where the joint PDF of state vector $\mathbf{x}_k$ and measurement vector $\mathbf{z}_k$ is formulated as

$$p(\mathbf{x}_k, \mathbf{z}_k|\mathbf{z}_{1:k-1}) = p(\mathbf{z}_k|\mathbf{x}_k) p(\mathbf{x}_k|\mathbf{z}_{1:k-1}) \tag{4}$$

where $p(\mathbf{z}_k|\mathbf{x}_k)$ is the measurement likelihood PDF, and the likelihood function is formulated as

$$\begin{aligned} p(\mathbf{z}_k|\mathbf{z}_{1:k-1}) &= \int p(\mathbf{x}_k, \mathbf{z}_k|\mathbf{z}_{1:k-1}) d\mathbf{x}_k \\ &= \int p(\mathbf{z}_k|\mathbf{x}_k) p(\mathbf{x}_k|\mathbf{z}_{1:k-1}) d\mathbf{x}_k \end{aligned} \tag{5}$$

For nonlinear system, the closed-form solution for posterior PDF is usually unavailable since the integrals in (2) and (5) cannot be calculated analytically. The GAFs are the most common approaches to calculate the equations formulated as (2)–(5) approximately based on the assumption that the joint PDF of state vector $\mathbf{x}_k$ and measurement vector $\mathbf{z}_k$ is

approximated as Gaussian [38], that is

$$\begin{aligned} &p(\mathbf{x}_k, \mathbf{z}_k|\mathbf{z}_{1:k-1}) \\ &\quad\approx \hat{p}(\mathbf{x}_k, \mathbf{z}_k|\mathbf{z}_{1:k-1}) \\ &\quad= \mathrm{N}\left(\begin{bmatrix}\mathbf{x}_k \\ \mathbf{z}_k\end{bmatrix}; \begin{bmatrix}\hat{\mathbf{x}}_{k|k-1} \\ \hat{\mathbf{z}}_{k|k-1}\end{bmatrix}, \begin{bmatrix}\mathbf{P}_{k|k-1} & \mathbf{P}^{xz}_{k|k-1} \\ \left(\mathbf{P}^{xz}_{k|k-1}\right)^T & \mathbf{P}^{zz}_{k|k-1}\end{bmatrix}\right) \end{aligned} \tag{6}$$

where $\hat{\mathbf{x}}_{k|k-1}$ and $\mathbf{P}_{k|k-1}$ present the first two moments with respect to $p(\mathbf{x}_k|\mathbf{z}_{1:k-1})$. $\hat{\mathbf{z}}_{k|k-1}$ and $\mathbf{P}^{zz}_{k|k-1}$ present the first two moments with respect to $p(\mathbf{z}_k|\mathbf{z}_{1:k-1})$, and $\mathbf{P}^{xz}_{k|k-1}$ presents the cross covariance matrix between state vector $\mathbf{x}_k$ and measurement vector $\mathbf{z}_k$.

According to the Bayesian rule, the posterior PDF $p(\mathbf{x}_k|\mathbf{z}_{1:k})$ can also be approximated as Gaussian based on the above-mentioned assumption. To evaluate the approximation accuracy of GAFs, the Kullback–Leibler divergence (KLD) $\mathrm{D}(p, \hat{p})$ between $p(\mathbf{x}_k, \mathbf{z}_k|\mathbf{z}_{1:k-1})$ and $\hat{p}(\mathbf{x}_k, \mathbf{z}_k|\mathbf{z}_{1:k-1})$ is calculated [21]–[34]

$$\begin{aligned} &\mathrm{D}(p, \hat{p}) \\ &= \left[\log\left(\mid \mathbf{I} + \mathbf{R}_k^{-1}\left(\mathbf{P}^{zz}_{k|k-1} - \mathbf{R}_k\right.\right.\right. \\ &\quad \left.\left.\left. - \left(\mathbf{P}^{xz}_{k|k-1}\right)^T\left(\mathbf{P}_{k|k-1}\right)^{-1}\mathbf{P}^{xz}_{k|k-1}\right) \mid\right)\right]/2 \\ &= \left[\log\left(\mid \mathbf{R}_k^{-1}\left(\mathbf{P}^{zz}_{k|k-1} - \left(\mathbf{P}^{xz}_{k|k-1}\right)^T\left(\mathbf{P}_{k|k-1}\right)^{-1}\mathbf{P}^{xz}_{k|k-1}\right) \mid\right)\right]/2 \end{aligned} \tag{7}$$

where $\mathbf{I}$ is the m-order unit matrix. It is clearly informed by (7) that $\mathrm{D}(p, \hat{p})$ increases as $\mathbf{R}_k$ decreases or $\mathbf{P}_{k|k-1}$ increases, which means that the standard GAFs may perform poorly in the situation with large prior uncertainty but high measurement accuracy. The use of PGAF has proven to be a powerful methodology for dealing with this problem.

Under the framework of PGAF, the time update phase has the identical form with standard GAFs, while in the measurement update phase, the measurement likelihood PDF is evolved gradually. In terms of Bayesian rule, the posterior PDF can be formulated as follows [33], [35], [36]:

$$p(\mathbf{x}_k|\mathbf{z}_{1:k}) \propto p(\mathbf{x}_k|\mathbf{z}_{1:k-1}) \prod_{\tau=1}^{N}\left[p\left(\mathbf{z}_k|\mathbf{x}_k^\tau\right)\right]^\Delta \tag{8}$$

where $[p(\mathbf{z}_k|\mathbf{x}_k^\tau)]^\Delta$ is the progressive measurement likelihood function, τ represents the recursion index, N represents the total recursion times, Δ represents the step size during the progressive process, and $\mathbf{x}_k^\tau$ represents the intermediate state vector at the τth progressive step.

By assuming each intermediate progressive joint PDFs of state and measurement as Gaussian, the intermediate one-step predicted PDFs $p(\mathbf{x}_k^\tau|\mathbf{z}_{1:k}^{\tau-1})$ and measurement likelihood PDFs $p(\mathbf{z}_k|\mathbf{x}_k^\tau)$ can be formulated as Gaussian distribution as follows:

$$p\left(\mathbf{x}_k^\tau|\mathbf{z}_{1:k}^{\tau-1}\right) = \mathrm{N}\left(\mathbf{x}_k^\tau; \hat{\mathbf{x}}_{k|k}^{\tau-1}, \mathbf{P}_{k|k}^{\tau-1}\right) \tag{9}$$

$$p\left(\mathbf{z}_k|\mathbf{x}_k^\tau\right) = \mathrm{N}\left(\mathbf{z}_k; \mathbf{h}_k\left(\mathbf{x}_k^\tau\right), \mathbf{R}_k\right) \tag{10}$$

where $\hat{\mathbf{x}}_{k|k}^\tau$ represents the estimate of $\mathbf{x}_k^\tau$, $\mathbf{z}_{1:k}^\tau$ represents the progressively included measurements' information, and $\mathbf{P}_{k|k}^\tau$ represents the estimated error covariance matrix of $\hat{\mathbf{x}}_{k|k}^\tau$ at the τth progressive step.

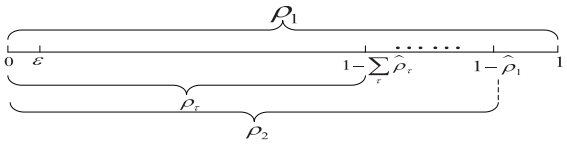

Fig. 1. Sketch map of progressive measurement update.

However, under the framework of the existing PGAF, the progressive step size is chosen as an invariant constant, namely, $\Delta = 1/N$, and the selection of that depends heavily upon the engineering experience. Therefore, the engineering practicality of the existing PGAF is dramatically degenerated because of the lacking of powerful theoretical foundations for the selections of optimal step size. Apart from that, the inevitable integral approximation errors will be accumulated as a result of the repeatedly approximated computations of the Gaussian weighted integrals, which can be modeled as additional pseudo-measurement noise. An inaccurate MNCM is often induced by the integral approximation errors, the moderately time-varying practical environment, and other non-modeling errors. For example, in the tightly coupled GNSS/INS integration applications, the measurement noises of pseudorange and pseudorange rate are easily disturbed by the multi-path reflections and bad weather conditions. To address the problems mentioned earlier, the VS-PGAF is proposed in this article.

III. Main Results

The VS-PGAF is developed in this section, where the intermediate state vector $\mathbf{x}_k^\tau$, the variable step size ρ_τ, as well as the inaccurate MNCM $\mathbf{R}_k^\tau$ are jointly estimated based on the VB method. The inaccurate MNCM is often caused by the moderately time-varying practical environment, the integral approximation errors, and other non-modeling errors. Under this framework, the intermediate measurement likelihood PDF and posterior PDF can be rewritten as follows:

$$p\left(\mathbf{z}_k|\mathbf{x}_k^\tau\right) = \mathrm{N}\left(\mathbf{z}_k; \mathbf{h}_k(\mathbf{x}_k^\tau), \mathbf{R}_k\right) \tag{11}$$

$$p(\mathbf{x}_k|\mathbf{z}_{1:k}) \propto p(\mathbf{x}_k|\mathbf{z}_{1:k-1}) \prod_{\tau=1}^{N}\left[p\left(\mathbf{z}_k|\mathbf{x}_k^\tau\right)\right]^{\rho_\tau} \tag{12}$$

where $\sum_{\tau=1}^N \rho_\tau = 1$. The sketch map of the progressive measurement update process is shown in Fig. 1. According to the proposed optimal step sizes' selection strategy, the first optimal step size is chosen from the interval $(0, 1]$, i.e., $\rho_1 \in (0, 1]$. Similarly, the optimal step size at the τth step satisfies $\rho_\tau \in (0, \eta_\tau]$, where $\eta_\tau = 1 - \sum_{j=1}^{\tau-1}\rho_j$, and the optimal step size ρ_τ will be variational inferred online. When the remaining measurement information reached the ultimate threshold, namely, $\eta_\tau < \varepsilon$, it will be absorbed at the last recursion loop.

A. Choices of Prior Distributions

For the purpose of inferring the intermediate state vector $\mathbf{x}_k^\tau$, the variable step size ρ_τ, as well as the inaccurate MNCM $\mathbf{R}_k^\tau$ jointly, the conjugate prior distributions need to be selected

primarily. In Bayesian statistics, the IG distribution usually arises as the conjugate prior distribution for the unknown variance of Gaussian distribution. The IG distribution of positive random variable χ is formulated as $\mathrm{IG}(\chi;\alpha,\beta) = (\beta^{\alpha}/\Gamma(\alpha))(1/\chi)^{\alpha+1}\exp(-\beta/\chi)$ with shape parameter α and scale parameter β, where $\Gamma(.)$ denotes the gamma function. $\mathbf{R}_k^{\tau} = \mathrm{diag}[(\sigma_{k,1}^{\tau})^2,\ldots,(\sigma_{k,m}^{\tau})^2]$, where $(\sigma_{k,j}^{\tau})^2$ is the jth diagonal element of $\mathbf{R}_k^{\tau}$. The prior distribution of $(\sigma_{k,j}^{\tau})^2$ can be formulated as follows:

$$p\big((\sigma_{k,j}^{\tau})^2|\mathbf{z}_{1:k}^{\tau-1}\big) = \mathrm{IG}\big((\sigma_{k,j}^{\tau})^2;\alpha_{k,j}^{\tau-1},\beta_{k,j}^{\tau-1}\big) \tag{13}$$

and meanwhile, the prior distribution of $\mathbf{R}_k^{\tau}$ can be formulated as

$$p\big(\mathbf{R}_k^{\tau}|\mathbf{z}_{1:k}^{\tau-1}\big) = \prod_{j=1}^{m}\mathrm{IG}\big((\sigma_{k,j}^{\tau})^2;\alpha_{k,j}^{\tau-1},\beta_{k,j}^{\tau-1}\big). \tag{14}$$

Remark 1: In Bayesian statistics, the IG distribution is always selected as the conjugate prior for the high-dimensional and diagonal covariance matrix of Gaussian. However, for the low- and medium-dimensional or nondiagonal covariance matrix of Gaussian, choosing inverse Wishart (IW) distribution as the conjugate prior will be more appropriate [39]. In the tightly coupled GNSS/INS integration applications, the MNCM is high-dimensional and diagonal, and therefore, choosing IG distribution as the conjugate prior presents better numerical stability than the IW distribution.

The variable step size ρ_{τ} is assumed to satisfy uniform distribution prior, that is

$$p\big(\rho_{\tau}|\mathbf{z}_{1:k}^{\tau-1}\big) = \mathrm{U}(\rho_{\tau};0,\eta_{\tau}) \tag{15}$$

where $\mathrm{U}(\cdot;b,d)$ denotes the uniform distribution on the interval $[b,d]$ and η_{τ} satisfies $\eta_{\tau} = 1-\sum_{j=1}^{\tau-1}\rho_j$.

B. Variational Approximations of Posterior PDFs

In order to infer the intermediate state $\mathbf{x}_k^{\tau}$, the variable step size ρ_{τ}, as well as the inaccurate MNCM $\mathbf{R}_k^{\tau}$ jointly, the joint posterior PDF $p(\mathbf{x}_k^{\tau},\rho_{\tau},\mathbf{R}_k^{\tau}|\mathbf{z}_{1:k})$ should be computed primarily. An analytic solution for such a joint posterior PDF is always unavailable, and therefore, the VB method is employed to look for a suboptimal approximation for the joint posterior PDF, that is

$$p\big(\mathbf{x}_k^{\tau},\rho_{\tau},\mathbf{R}_k^{\tau}|\mathbf{z}_{1:k}\big) \approx q\big(\mathbf{x}_k^{\tau}\big)q(\rho_{\tau})q\big(\mathbf{R}_k^{\tau}\big) \tag{16}$$

the approximate posterior PDFs $q(\mathbf{x}_k^{\tau})$, $q(\rho_{\tau})$, $q(\mathbf{R}_k^{\tau})$ can be obtained by solving the following equation [41], [42]:

$$\begin{aligned}&\big\{q\big(\mathbf{x}_k^{\tau}\big),q(\rho_{\tau}),q\big(\mathbf{R}_k^{\tau}\big)\big\}\\&\quad=\arg\min\mathbf{D}\big(q\big(\mathbf{x}_k^{\tau}\big)q(\rho_{\tau})q\big(\mathbf{R}_k^{\tau}\big)\big\|p\big(\mathbf{x}_k^{\tau},\rho_{\tau},\mathbf{R}_k^{\tau}|\mathbf{z}_{1:k}\big)\big)\end{aligned} \tag{17}$$

where $\mathbf{D}(q(x)||p(x)) \triangleq \int q(x)\log(q(x)/p(x))dx$ represents the KLD between the approximate PDF $q(x)$ and the real PDF $p(x)$. According to the VB theory, the optimal solution for (17) satisfies the following equation:

$$\log q(\theta) = \mathrm{E}_{\Phi^{(-\theta)}}[\log p(\Phi,\mathbf{z}_{1:k})] + c_{\theta} \tag{18}$$

where $\Phi \triangleq \{\mathbf{x}_k^{\tau},\rho_{\tau},\mathbf{R}_k^{\tau}\}$. $\log(\cdot)$ denotes the logarithmic operation and $\mathrm{E}_{(\theta)}[\cdot]$ denotes the expectation operation with respect to θ. $\Phi^{(-\theta)}$ is a subset of Φ satisfying $\{\theta\}\bigcup\Phi^{(-\theta)} = \Phi$. c_{θ} is a constant independent of θ. To address the intercoupling among the variational parameters of $q(\mathbf{x}_k^{\tau})$, $q(\rho_{\tau})$, and $q(\mathbf{R}_k^{\tau})$, fixed-point iterations are adopted to solve (18) [42]. By this method, the approximate posterior PDF $q(\theta)$ is computed as $q^{(i+1)}(\theta)$ at the $i+1$th iteration based on the previous approximate PDF $q^{(i)}(\Phi^{(-\theta)})$. Consequently, the VB approach is sensitive to the initial value, and the iterations will converge to a local optimum of (18).

In terms of Bayesian rule, the joint PDF $p(\Phi,\mathbf{z}_{1:k})$ can be factored as follows:

$$\begin{aligned}&p(\Phi,\mathbf{z}_{1:k})\\&\quad=c(\tau)p\big(\mathbf{x}_k^{\tau}|\mathbf{z}_{1:k}^{\tau-1}\big)p\big(\mathbf{R}_k^{\tau}|\mathbf{z}_{1:k}^{\tau-1}\big)p\big(\rho_{\tau}|\mathbf{z}_{1:k}^{\tau-1}\big)\big[p\big(\mathbf{z}_k|\mathbf{x}_k^{\tau}\big)\big]^{\rho_{\tau}}\end{aligned} \tag{19}$$

where $c(\tau)$ denotes the normalization constant. Substituting (9), (11), (14), and (15) into (19), we obtain

$$\begin{aligned}&p(\Phi,\mathbf{z}_{1:k})\\&\quad=c(\tau)\mathrm{N}\big(\mathbf{x}_k^{\tau};\hat{\mathbf{x}}_{k|k}^{\tau-1},\mathbf{p}_{k|k}^{\tau-1}\big)\prod_{j=1}^{m}\mathrm{IG}\big((\sigma_{k,j}^{\tau})^2;\alpha_{k,j}^{\tau-1},\beta_{k,j}^{\tau-1}\big)\\&\qquad\times\mathrm{U}(\rho_{\tau};0,\eta_{\tau})\mathrm{N}\big(\mathbf{z}_k;\mathbf{h}_k\big(\mathbf{x}_k^{\tau}\big),\mathbf{R}_k^{\tau}/\rho_{\tau}\big).\end{aligned} \tag{20}$$

Exploiting (20) and making a logarithmic operation, we have

$$\begin{aligned}&\log p(\Phi,\mathbf{z}_{1:k})\\&\quad=0.5m\log\rho_{\tau}-0.5\big(\mathbf{x}_k^{\tau}-\hat{\mathbf{x}}_{k|k}^{\tau-1}\big)^T\big(\mathbf{P}_{k|k}^{\tau-1}\big)^{-1}\big(\mathbf{x}_k^{\tau}-\hat{\mathbf{x}}_{k|k}^{\tau-1}\big)\\&\qquad-0.5\rho_{\tau}\big(\mathbf{z}_k-\mathbf{h}_k\big(\mathbf{x}_k^{\tau}\big)\big)^T\big(\mathbf{R}_k^{\tau}\big)^{-1}\big(\mathbf{z}_k-\mathbf{h}_k\big(\mathbf{x}_k^{\tau}\big)\big)\\&\qquad-\sum_{j=1}^{m}\left[\big(\alpha_{k,j}^{\tau-1}+1.5\big)\log\big(\sigma_{k,j}^{\tau}\big)^2+\frac{\beta_{k,j}^{\tau-1}}{\big(\sigma_{k,j}^{\tau}\big)^2}\right]+c_{\Phi}\end{aligned} \tag{21}$$

where c_{Φ} is the constant independent of Φ. Equation (21) can be further rewritten as

$$\begin{aligned}&\log p(\Phi,\mathbf{z}_{1:k})\\&\quad=0.5m\log\rho_{\tau}-0.5\big(\mathbf{x}_k^{\tau}-\hat{\mathbf{x}}_{k|k}^{\tau-1}\big)^T\big(\mathbf{P}_{k|k}^{\tau-1}\big)^{-1}\big(\mathbf{x}_k^{\tau}-\hat{\mathbf{x}}_{k|k}^{\tau-1}\big)\\&\qquad-\sum_{j=1}^{m}\log\big(\sigma_{k,j}^{\tau}\big)^2\big(\alpha_{k,j}^{\tau-1}+1.5\big)\\&\qquad-\sum_{j=1}^{m}\frac{1}{\big(\sigma_{k,j}^{\tau}\big)^2}\big(\beta_{k,j}^{\tau-1}+0.5\rho_{\tau}\big(\mathbf{z}_{k,j}-\mathbf{h}_{k,j}\big(\mathbf{x}_k^{\tau}\big)\big)^2\big)+c_{\Phi}\end{aligned} \tag{22}$$

where $\mathbf{z}_{k,j}$ and $\mathbf{h}_{k,j}(\mathbf{x}_k^{\tau})$ denote the jth element of vector $\mathbf{z}_k$ and $\mathbf{h}_k(\mathbf{x}_k^{\tau})$, respectively. Both (21) and (22) will play important roles in the following derivation.

Substituting $\theta=\rho_{\tau}$ in (18) and utilizing (21), we yield

$$\begin{aligned}\log q^{i+1}(\rho_{\tau}) &= 0.5m\log\rho_{\tau}\\&\quad-0.5\rho_{\tau}\mathrm{tr}\big(\mathbf{U}_k^{\tau(i)}\mathrm{E}^i\big[\big(\mathbf{R}_k^{\tau}\big)^{-1}\big]\big)+c_{\rho}\end{aligned} \tag{23}$$

where $\mathbf{U}_k^{\tau(i)}$ can be given by

$$\mathbf{U}_k^{\tau(i)} = \mathrm{E}^i\big[\big(\mathbf{z}_k-\mathbf{h}_k\big(\mathbf{x}_k^{\tau}\big)\big)\big(\mathbf{z}_k-\mathbf{h}_k\big(\mathbf{x}_k^{\tau}\big)\big)^T\big]. \tag{24}$$

Thus, $q^{i+1}(\rho_\tau)$ can be updated as gamma distribution with shape parameter $\varphi^{\tau(i+1)}$ and rate parameter $\psi^{\tau(i+1)}$

$$q^{i+1}(\rho_\tau) = \mathrm{G}(\rho_\tau; \varphi^{\tau(i+1)}, \psi^{\tau(i+1)}) \tag{25}$$

where $\mathrm{G}(\cdot; \varphi, \psi)$ denotes the gamma distribution. Considering that ρ_τ is meaningful if and only if $\rho_\tau \in (0, 1]$, thus the gamma PDF is truncated. $\varphi^{\tau(i+1)}$ and $\psi^{\tau(i+1)}$ can be formulated as

$$\varphi^{\tau(i+1)} = 0.5m + 1 \tag{26}$$

$$\psi^{\tau(i+1)} = 0.5\mathrm{tr}\big(\mathbf{U}_k^{\tau(i)}\mathrm{E}^i\big[\big(\mathbf{R}_k^\tau\big)^{-1}\big]\big). \tag{27}$$

Let $\theta = (\sigma_{k,j}^\tau)^2$, and utilizing (22) in (18), we obtain

$$q^{i+1}\big(\big(\sigma_{k,j}^\tau\big)^2\big) = -\log\big(\sigma_{k,j}^\tau\big)^2\big(\alpha_{k,j}^{\tau-1} + 1.5\big) - \frac{1}{\big(\sigma_{k,j}^\tau\big)^2} \times \big(\beta_{k,j}^{\tau-1} + 0.5\mathrm{E}^{i+1}[\rho_\tau]\big[\mathbf{U}_k^{\tau(i)}\big]_{j,j}\big) + c_\sigma \tag{28}$$

where $[\mathbf{U}_k^{\tau(i)}]_{j,j}$ denotes the jth diagonal element of matrix $\mathbf{U}_k^{\tau(i)}$. Thus, $q^{i+1}((\sigma_{k,j}^\tau)^2)$ can be updated as

$$q^{i+1}\big(\big(\sigma_{k,j}^\tau\big)^2\big) = \mathrm{IG}\big(\big(\sigma_{k,j}^\tau\big)^2; \alpha_{k,j}^{\tau(i+1)}, \beta_{k,j}^{\tau(i+1)}\big) \tag{29}$$

where the shape parameter $\alpha_{k,j}^{\tau(i+1)}$ and scale parameter $\beta_{k,j}^{\tau(i+1)}$ are updated as follows:

$$\alpha_{k,j}^{\tau(i+1)} = \alpha_{k,j}^{\tau-1} + 0.5 \tag{30}$$

$$\beta_{k,j}^{\tau(i+1)} = \beta_{k,j}^{\tau-1} + 0.5\mathrm{E}^{i+1}[\rho_\tau]\big[\mathbf{U}_k^{\tau(i)}\big]_{j,j}. \tag{31}$$

Let $\theta = \mathbf{x}_k^\tau$, and utilizing (21) in (18), we obtain

$$\log q^{i+1}\big(\mathbf{x}_k^\tau\big) = -0.5\big(\mathbf{x}_k^\tau - \hat{\mathbf{x}}_{k|k}^{\tau-1}\big)^T\big(\mathbf{P}_{k|k}^{\tau-1}\big)^{-1}\big(\mathbf{x}_k^\tau - \hat{\mathbf{x}}_{k|k}^{\tau-1}\big) - 0.5\big(\mathbf{z}_k - \mathbf{h}_k\big(\mathbf{x}_k^\tau\big)\big)^T\big(\tilde{\mathbf{R}}_k^{\tau(i+1)}\big)^{-1}\big(\mathbf{z}_k - \mathbf{h}_k\big(\mathbf{x}_k^\tau\big)\big) + c_x \tag{32}$$

where

$$\tilde{\mathbf{R}}_k^{\tau(i+1)} = \mathrm{E}^{i+1}[\mathbf{R}_k^\tau]/\mathrm{E}^{i+1}[\rho^\tau]. \tag{33}$$

According to the property of IG distribution, $\mathrm{E}^{i+1}[\mathbf{R}_k^\tau]$ can be computed as

$$\mathrm{E}^{i+1}[\mathbf{R}_k^\tau] = \mathrm{diag}\big[\beta_{k,1}^{\tau(i+1)}/\alpha_{k,1}^{\tau(i+1)}, \ldots, \beta_{k,m}^{\tau(i+1)}/\alpha_{k,m}^{\tau(i+1)}\big]. \tag{34}$$

Since the PDF $q^{i+1}(\rho^\tau)$ satisfies a truncated gamma PDF, the definition of integral is employed to calculate $\mathrm{E}^{i+1}[\rho^\tau]$, namely

$$\mathrm{E}^{i+1}[\rho^\tau] = \int_0^{\eta_\tau} \rho^\tau \mathrm{G}(\rho_\tau; \varphi^{\tau(i+1)}, \psi^{\tau(i+1)})d\rho^\tau \approx \frac{\eta_\tau^2}{\mathcal{L}^2}\sum_{\kappa=1}^{\mathcal{L}} \kappa\mathrm{G}\left(\frac{\kappa\eta_\tau}{\mathcal{L}}; \varphi^{\tau(i+1)}, \psi^{\tau(i+1)}\right) \tag{35}$$

where the integral interval $(0, \eta_\tau]$ is equally divided into $\mathcal{L}$ parts.

Using (32)–(34), $q^{i+1}(\mathbf{x}_k^\tau)$ can be formulated as

$$q^{i+1}\big(\mathbf{x}_k^\tau\big) \propto \mathrm{N}\big(\mathbf{z}_k; \mathbf{h}_k\big(\mathbf{x}_k^\tau\big), \tilde{\mathbf{R}}_k^{\tau(i+1)}\big)\mathrm{N}\big(\mathbf{x}_k^\tau; \hat{\mathbf{x}}_{k|k}^{\tau-1}, \mathbf{P}_{k|k}^{\tau-1}\big). \tag{36}$$

Therefore, the PDF $q^{i+1}(\mathbf{x}_k^\tau)$ can be approximated as Gaussian $\mathrm{N}(\mathbf{z}_k; \mathbf{h}_k(\mathbf{x}_k^\tau), \tilde{\mathbf{R}}_k^{\tau(i+1)})$, that is

$$q^{i+1}\big(\mathbf{x}_k^\tau\big) = \mathrm{N}\big(\mathbf{x}_k^\tau; \hat{\mathbf{x}}_{k|k}^{\tau(i+1)}, \mathbf{P}_{k|k}^{\tau(i+1)}\big) \tag{37}$$

where $\hat{\mathbf{x}}_{k|k}^{\tau(i+1)}$ and $\mathbf{P}_{k|k}^{\tau(i+1)}$ denote the first two moments with respect to $q^{i+1}(\mathbf{x}_k^\tau)$ and can be formulated as follows:

$$\mathbf{K}_k^{\tau(i+1)} = \mathbf{P}_{k|k}^{xz,\tau}\big(\mathbf{P}_{k|k}^{zz,\tau(i+1)}\big)^{-1} \tag{38}$$

$$\hat{\mathbf{x}}_{k|k}^{\tau(i+1)} = \hat{\mathbf{x}}_{k|k}^{\tau-1} + \mathbf{K}_k^{\tau(i+1)}\big(\mathbf{z}_k - \hat{\mathbf{z}}_{k|k}^\tau\big) \tag{39}$$

$$\mathbf{P}_{k|k}^{\tau(i+1)} = \mathbf{P}_{k|k}^{\tau-1} - \mathbf{K}_k^{\tau(i+1)}\mathbf{P}_{k|k}^{zz,\tau(i+1)}\big(\mathbf{K}_k^{\tau(i+1)}\big)^T \tag{40}$$

where $\mathbf{K}_k^{\tau(i+1)}$ denotes the progressive filtering gain. The corresponding vectors and matrices are derived as follows:

$$\begin{aligned}\hat{\mathbf{z}}_{k|k}^\tau &= \int\int \mathbf{z}_k p\big(\mathbf{x}_k^\tau, \mathbf{z}_k|\mathbf{z}_{1:k}^{\tau-1}\big)d\mathbf{z}_k d\mathbf{x}_k^\tau \\ &= \int\left[\int \mathbf{z}_k p\big(\mathbf{z}_k|\mathbf{x}_k^\tau\big)d\mathbf{z}_k\right] p\big(\mathbf{x}_k^\tau|\mathbf{z}_{1:k}^{\tau-1}\big)d\mathbf{x}_k^\tau \\ &= \int \mathbf{h}_k\big(\mathbf{x}_k^\tau\big)p\big(\mathbf{x}_k^\tau|\mathbf{z}_{1:k}^{\tau-1}\big)d\mathbf{x}_k^\tau \\ &\approx \int \mathbf{h}_k\big(\mathbf{x}_k^\tau\big)\mathrm{N}\big(\mathbf{x}_k^\tau; \hat{\mathbf{x}}_{k|k}^{\tau-1}, \mathbf{P}_{k|k}^{\tau-1}\big)d\mathbf{x}_k^\tau\end{aligned} \tag{41}$$

$$\begin{aligned}\mathbf{P}_{k|k}^{zz,\tau(i+1)} &= \int\int \big(\mathbf{z}_k - \hat{\mathbf{z}}_{k|k}^\tau\big)\big(\mathbf{z}_k - \hat{\mathbf{z}}_{k|k}^\tau\big)^T p\big(\mathbf{x}_k^\tau, \mathbf{z}_k|\mathbf{z}_{1:k}^{\tau-1}\big)d\mathbf{z}_k d\mathbf{x}_k^\tau \\ &= \int\left[\int \mathbf{z}_k\mathbf{z}_k^T p\big(\mathbf{z}_k|\mathbf{x}_k^\tau\big)d\mathbf{z}_k\right] p\big(\mathbf{x}_k^\tau|\mathbf{z}_{1:k}^{\tau-1}\big)d\mathbf{x}_k^\tau - \big(\hat{\mathbf{z}}_{k|k}^\tau\big)\big(\hat{\mathbf{z}}_{k|k}^\tau\big)^T \\ &= \int \mathbf{h}_k\big(\mathbf{x}_k^\tau\big)\mathbf{h}_k^T\big(\mathbf{x}_k^\tau\big)p\big(\mathbf{x}_k^\tau|\mathbf{z}_{1:k}^{\tau-1}\big)d\mathbf{x}_k^\tau + \tilde{\mathbf{R}}_k^{\tau(i+1)} - \big(\hat{\mathbf{z}}_{k|k}^\tau\big)\big(\hat{\mathbf{z}}_{k|k}^\tau\big)^T \\ &\approx \int \mathbf{h}_k\big(\mathbf{x}_k^\tau\big)\mathbf{h}_k^T\big(\mathbf{x}_k^\tau\big)\mathrm{N}\big(\mathbf{x}_k^\tau; \hat{\mathbf{x}}_{k|k}^{\tau-1}, \mathbf{P}_{k|k}^{\tau-1}\big)d\mathbf{x}_k^\tau + \tilde{\mathbf{R}}_k^{\tau(i+1)} \\ &\quad - \big(\hat{\mathbf{z}}_{k|k}^\tau\big)\big(\hat{\mathbf{z}}_{k|k}^\tau\big)^T\end{aligned} \tag{42}$$

$$\begin{aligned}\mathbf{P}_{k|k}^{xz,\tau} &= \int\int \big(\mathbf{x}_k^\tau - \hat{\mathbf{x}}_{k|k}^{\tau-1}\big)\big(\mathbf{z}_k - \hat{\mathbf{z}}_{k|k}^\tau\big)^T p\big(\mathbf{x}_k^\tau, \mathbf{z}_k|\mathbf{z}_{1:k}^{\tau-1}\big)d\mathbf{z}_k d\mathbf{x}_k^\tau \\ &= \int \mathbf{x}_k^\tau\left[\int \mathbf{z}_k^T p\big(\mathbf{z}_k|\mathbf{x}_k^\tau\big)d\mathbf{z}_k\right] p\big(\mathbf{x}_k^\tau|\mathbf{z}_{1:k}^{\tau-1}\big)d\mathbf{x}_k^\tau - \hat{\mathbf{x}}_{k|k}^{\tau-1}\big(\hat{\mathbf{z}}_{k|k}^\tau\big)^T \\ &= \int \mathbf{x}_k^\tau\mathbf{h}_k^T\big(\mathbf{x}_k^\tau\big)p\big(\mathbf{x}_k^\tau|\mathbf{z}_{1:k}^{\tau-1}\big)d\mathbf{x}_k^\tau - \hat{\mathbf{x}}_{k|k}^{\tau-1}\big(\hat{\mathbf{z}}_{k|k}^\tau\big)^T \\ &\approx \int \mathbf{x}_k^\tau\mathbf{h}_k^T\big(\mathbf{x}_k^\tau\big)\mathrm{N}\big(\mathbf{x}_k^\tau; \hat{\mathbf{x}}_{k|k}^{\tau-1}, \mathbf{P}_{k|k}^{\tau-1}\big)d\mathbf{x}_k - \hat{\mathbf{x}}_{k|k}^{\tau-1}\big(\hat{\mathbf{z}}_{k|k}^\tau\big)^T.\end{aligned} \tag{43}$$

The progressive process will be stopped once the remaining progressive quantity η_τ is smaller than the threshold value ε, and the left measurement information will be assimilated at the ultimate recursion. After the Λth recursions, we finally obtain $\hat{\mathbf{x}}_{k|k} = \hat{\mathbf{x}}_{k|k}^\Lambda$ and $\mathbf{P}_{k|k} = \mathbf{P}_{k|k}^\Lambda$.

Remark 2: To balance the computational complexity and the estimation accuracy, the fixed-point iterations loops are executed only when the following constraint is satisfied:

$$\mathrm{Norm}(\Phi^{(i+1)}, \Phi^{(i)}) > \zeta \tag{44}$$

where $\mathrm{Norm}(\cdot, \cdot)$ represents the 2-norm distance and threshold value ζ in this article is set empirically as 10^{-6}.

In the framework of PGAFs, the initial values of progressive measurement update are normally chosen as the corresponding prior outcomes, that is

$$\hat{\mathbf{x}}_{k|k}^{0} = \hat{\mathbf{x}}_{k|k-1} \qquad \mathbf{P}_{k|k}^{0} = \mathbf{P}_{k|k-1}. \tag{45}$$

Meanwhile, we have

$$\alpha_{k|k,j}^{0} = \alpha_{k|k-1,j} + 0.5 \qquad \beta_{k|k,j}^{0} = \beta_{k|k-1,j}. \tag{46}$$

C. Time Update

Under the framework of PGAF, the time update has the identical form with the standard GAFs. According to (2), the predicted state estimation $\hat{\mathbf{x}}_{k|k-1}$ and predicted error covariance matrix $\mathbf{P}_{k|k-1}$ can be formulated as follows:

$$\begin{aligned}
&\hat{\mathbf{x}}_{k|k-1} \\
&= \int \mathbf{x}_k\, p(\mathbf{x}_k|\mathbf{z}_{1:k-1}) d\mathbf{x}_k \\
&= \int \mathbf{f}_{k-1}(\mathbf{x}_{k-1})\, p(\mathbf{x}_{k-1}|\mathbf{z}_{1:k-1}) d\mathbf{x}_{k-1} \\
&\approx \int \mathbf{f}_{k-1}(\mathbf{x}_{k-1}) \mathrm{N}(\mathbf{x}_{k-1}; \hat{\mathbf{x}}_{k-1|k-1}, \mathbf{P}_{k-1|k-1}) d\mathbf{x}_{k-1}
\end{aligned} \tag{47}$$

$$\begin{aligned}
&\mathbf{P}_{k|k-1} \\
&= \int \mathbf{x}_k \mathbf{x}_k^T\, p(\mathbf{x}_k|\mathbf{z}_{1:k-1}) d\mathbf{x}_k - (\hat{\mathbf{x}}_{k|k-1})(\hat{\mathbf{x}}_{k|k-1})^T \\
&= \int \mathbf{f}_{k-1}(\mathbf{x}_{k-1}) \mathbf{f}_{k-1}^T(\mathbf{x}_{k-1})\, p(\mathbf{x}_{k-1}|\mathbf{z}_{1:k-1}) d\mathbf{x}_{k-1} \\
&\quad + \mathbf{Q}_{k-1} - (\hat{\mathbf{x}}_{k|k-1})(\hat{\mathbf{x}}_{k|k-1})^T \\
&\approx \int \mathbf{f}_{k-1}(\mathbf{x}_{k-1}) \mathbf{f}_{k-1}^T(\mathbf{x}_{k-1}) \mathrm{N}(\mathbf{x}_{k-1}; \hat{\mathbf{x}}_{k-1|k-1}, \mathbf{P}_{k-1|k-1}) d\mathbf{x}_{k-1} \\
&\quad + \mathbf{Q}_{k-1} - (\hat{\mathbf{x}}_{k|k-1})(\hat{\mathbf{x}}_{k|k-1})^T.
\end{aligned} \tag{48}$$

Furthermore, the time update parameters of MNCM should be determined. According to the Bayesian rule, the predicted PDF $p(\mathbf{R}_k|\mathbf{z}_{1:k-1})$ can be formulated as

$$p(\mathbf{R}_k|\mathbf{z}_{1:k-1}) = \int p(\mathbf{R}_k|\mathbf{R}_{k-1})\, p(\mathbf{R}_{k-1}|\mathbf{z}_{1:k-1}) d\mathbf{R}_{k-1} \tag{49}$$

where $p(\mathbf{R}_{k-1}|\mathbf{z}_{1:k-1})$ is the posterior PDF of MNCM at $k-1$ time and $p(\mathbf{R}_k|\mathbf{R}_{k-1})$ is the transition PDF. In practical applications, the transition model $p(\mathbf{R}_k|\mathbf{R}_{k-1})$ is hard to determine, and thus, in this article, considering that the MNCM is mildly time-varying in many practical applications, a discount factor $\varrho \in (0, 1]$ is utilized to illustrate the time-fluctuation level. Based on the previous posterior PDF and discount factor ϱ, the prior parameters are given by

$$\alpha_{k|k-1,j} = \varrho \alpha_{k-1,j} \tag{50}$$

$$\beta_{k|k-1,j} = \varrho \beta_{k-1,j}. \tag{51}$$

Given a nominal MNCM $\bar{\mathbf{R}}_0$, the proposed VS-PGAF is summarized in Table I, where M represents the ultimate number of fixed-point iterations and N_{VB} represents the preset maximum number of VB recursions.

IV. Application for Tightly Coupled GNSS/INS Integration

A. State Transition Model

In the tightly coupled GNSS/INS integration, the state vector is chosen as

$$\begin{aligned}
\mathbf{x} &= \begin{bmatrix} \Psi_{nb}^n & \delta\mathbf{v}_{nb}^n & \delta\mathbf{p}_b & \mathbf{b}_a & \mathbf{b}_g & \delta t_B & \delta t_D \end{bmatrix}^T \\
\delta\mathbf{p}_b &= [\delta L_b \quad \delta\rho_b \quad \delta h_b]^T
\end{aligned}$$

where $\mathbf{x} \in \mathbb{R}^{17}$. $\Psi_{nb}^n \in \mathbb{R}^3$ denotes the attitude error vector and $\delta\mathbf{v}_{nb}^n \in \mathbb{R}^3$ denotes the velocity error vector, both of which are projected in the north-east-down (END) navigation frame (n-frame). δL_b, $\delta\rho_b$, and δh_b are the latitude, longitude, and height errors, respectively, expressed as the position error vector $\delta\mathbf{p}_b$. $\mathbf{b}_a, \mathbf{b}_g \in \mathbb{R}^3$ are the bias vector of accelerometers and gyros projected in the body frame (b-frame). δt_B and δt_D are the pseudorange and pseudorange rate uncertainty caused by the clock offset and clock drift of receiver, respectively [25]. The differential state transition model is summarily formulated as follows:

$$\dot{\Psi}_{nb}^n = \delta\Omega_{ie}^n + \delta\Omega_{en}^n - \left(\Omega_{ie}^n + \Omega_{en}^n\right) \times \Psi_{nb}^n + \hat{\mathbf{C}}_b^n \mathbf{b}_g \tag{52}$$

$$\begin{aligned}
\delta\dot{\mathbf{v}}_{nb}^n = &\left(\hat{\mathbf{C}}_b^n \hat{\mathbf{f}}_{ib}^b\right) \times \Psi_{nb}^n - \left(2\delta\Omega_{ie}^n + \delta\Omega_{en}^n\right) \times \mathbf{v}_{nb}^n \\
&- \left(2\Omega_{ie}^n + \Omega_{en}^n\right) \times \delta\mathbf{v}_{nb}^n + \hat{\mathbf{C}}_b^n \mathbf{b}_a
\end{aligned} \tag{53}$$

$$\begin{cases}
\delta\dot{L}_b = \dfrac{\delta\mathbf{v}_{eb,N}^n}{\mathrm{R}_N + \hat{h}_b} - \dfrac{\delta\mathbf{v}_{eb,N}^n \delta h_b}{(\mathrm{R}_N + \hat{h}_b)^2} \\
\delta\dot{\rho}_b = \dfrac{\delta\mathbf{v}_{eb,E}^n \sec(\hat{L}_b)}{\mathrm{R}_E + \hat{h}_b} + \dfrac{\delta\mathbf{v}_{eb,E}^n \delta L_b \sin(\hat{L}_b)}{(\mathrm{R}_E + \hat{h}_b)\cos^2(\hat{L}_b)} \\
\qquad\qquad - \dfrac{\delta\mathbf{v}_{eb,E}^n \delta h_b}{(\mathrm{R}_E + \hat{h}_b)^2 \cos(\hat{L}_b)} \\
\delta\dot{h}_b = -\delta\mathbf{v}_{eb,D}^n
\end{cases} \tag{54}$$

$$\delta\dot{t}_B = \delta t_D + w_B \tag{55}$$

where symbol $\times$ represents the vector cross product operation. Ω_{ie}^n is the earth rotation angular rate vector with respect to the inertial frame (i-frame) presented in n-frame, which can be computed based on the estimated latitude. Ω_{en}^n is the relative rotation angular rate vector between the n-frame and the earth-centered earth-fixed frame (e-frame) presented in the n-frame and $\mathbf{v}_{nb}^n$ is the velocity vector of receiver presented in the n-frame, which can be easily calculated based on the outputs of inertial sensors and the estimated solution. $\delta\Omega_{ie}^n$ and $\delta\Omega_{en}^n$ are the corresponding error vectors, respectively. $\hat{\mathbf{C}}_b^n$ is the estimated rotational matrix from b-frame to n-frame. $\hat{\mathbf{f}}_{ib}^b$ denotes the specific force vector given by accelerometers and projected in b-frame. $\delta\mathbf{v}_{eb,N}^n$, $\delta\mathbf{v}_{eb,E}^n$, and $\delta\mathbf{v}_{eb,D}^n$ denote the component of $\delta\mathbf{v}_{eb}^n$ decomposed in the north, east, and down directions, respectively. $\hat{L}_b$, $\hat{\rho}_b$, and $\hat{h}_b$ present the estimated latitude, longitude, and height, respectively. R_N denotes the meridian radius and R_E denotes the transverse radius of the earth, both of them are known constant. w_B is considered as the zero mean Gaussian white noise.

Remark 3: The large prior uncertainty means the large one-step prediction error covariance matrix, just as (7) described. In the tightly coupled GNSS/INS integration,

TABLE I
IMPLEMENTATION PSEUDOCODE FOR THE PROPOSED VS-PGAF

Inputs: $\hat{\mathbf{x}}_{k-1|k-1}$, $\mathbf{P}_{k-1|k-1}$, $\mathbf{z}_k$, $\mathbf{f}_{k-1}(\cdot)$, $\mathbf{h}_k(\cdot)$, $\bar{\mathbf{R}}_{\mathbf{0}}$, ϱ, $\alpha_{k-1,j}$, $\beta_{k-1,j}$ $(j = 1 \dots m)$, N, N_{VB}
Time update:
1. $\hat{\mathbf{x}}_{k|k-1} \approx \int \mathbf{f}_{k-1}(\mathbf{x}_{k-1})\mathrm{N}(\mathbf{x}_{k-1}; \hat{\mathbf{x}}_{k-1|k-1}, \mathbf{P}_{k-1|k-1})d\mathbf{x}_{k-1}$
2. $\mathbf{P}_{k|k-1} \approx \int \mathbf{f}_{k-1}(\mathbf{x}_{k-1})\mathbf{f}_{k-1}^{T}(\mathbf{x}_{k-1})\mathrm{N}(\mathbf{x}_{k-1}; \hat{\mathbf{x}}_{k-1|k-1}, \mathbf{P}_{k-1|k-1})d\mathbf{x}_{k-1} + \mathbf{Q}_{k-1} - (\hat{\mathbf{x}}_{k|k-1})(\hat{\mathbf{x}}_{k|k-1})^{T}$
3. **for** $j = 1 : m$
$\alpha_{k|k-1,j} = \varrho\alpha_{k-1,j}, \quad \beta_{k|k-1,j} = \varrho\beta_{k-1,j}$
end for
Measurement update:
4. Initialization of progressive loop:
$\hat{\mathbf{x}}_{k|k}^{0} = \hat{\mathbf{x}}_{k|k-1}, \quad \mathbf{P}_{k|k}^{0} = \mathbf{P}_{k|k-1}$
for $j = 1 : m$
$\alpha_{k|k,j}^{0} = \alpha_{k|k-1,j} + 0.5, \quad \beta_{k|k,j}^{0} = \beta_{k|k-1,j}$
end for
for $\tau = 1 : N$
5. Initialization of fix-point iterations:
$\hat{\mathbf{x}}_{k|k}^{\tau(0)} = \hat{\mathbf{x}}_{k|k}^{\tau-1}, \quad \mathbf{P}_{k|k}^{\tau(0)} = \mathbf{P}_{k|k}^{\tau-1}, \quad \mathrm{E}^{0}[\mathbf{R}_k^{\tau}] = \bar{\mathbf{R}}_{\mathbf{0}}$
while $i \leq N_{VB}$ **AND** $\mathrm{Norm}(\mathbf{\Phi}^{(i)}, \mathbf{\Phi}^{(i-1)}) > \zeta$
Update $q^{i+1}(\rho_\tau) = \mathrm{G}(\rho_\tau; \varphi^{\tau(i+1)}, \psi^{\tau(i+1)})$ given $q^{i}(\mathbf{x}_k^{\tau})$ and $q^{i}((\sigma_{k,j}^{\tau})^2)$:
6. $\mathbf{U}_k^{\tau(i)} = \mathrm{E}^{i}[(\mathbf{z}_k - \mathbf{h}_k(\mathbf{x}_k^{\tau}))(\mathbf{z}_k - \mathbf{h}_k(\mathbf{x}_k^{\tau}))^{T}]$
7. $\varphi^{\tau(i+1)} = 0.5m + 1, \quad \psi^{\tau(i+1)} = 0.5\mathrm{tr}(\mathbf{U}_k^{\tau(i)}\mathrm{E}^{i}[(\mathbf{R}_k^{\tau})^{-1}])$
Update $q^{i+1}((\sigma_{k,j}^{\tau})^2) = \mathrm{IG}((\sigma_{k,j}^{\tau})^2; \alpha_{k,j}^{\tau(i+1)}, \beta_{k,j}^{\tau(i+1)})$ given $q^{i}(\mathbf{x}_k^{\tau})$ and $q^{i+1}(\rho_\tau)$:
8. $\alpha_{k,j}^{\tau(i+1)} = \alpha_{k,j}^{\tau-1} + 0.5, \quad \beta_{k,j}^{\tau(i+1)} = \beta_{k,j}^{\tau-1} + 0.5\mathrm{E}^{i+1}[\rho_\tau][\mathbf{U}_k^{\tau(i)}]_{j,j}$
Update $q^{i+1}(\mathbf{x}_k^{\tau}) = \mathrm{N}(\mathbf{x}_k^{\tau}; \hat{\mathbf{x}}_{k|k}^{\tau(i+1)}, \mathbf{P}_{k|k}^{\tau(i+1)})$ given $q^{i+1}(\mathbf{x}_k^{\tau})$ and $q^{i+1}(\rho_\tau)$:
9. Computed $\mathrm{E}^{i+1}[\mathbf{R}_k^{\tau}]$ and $E^{i+1}[\rho^{\tau}]$ by (34) and (35)
10. $\tilde{\mathbf{R}}_k^{\tau(i+1)} = \mathrm{E}^{i+1}[\mathbf{R}_k^{\tau}]/\mathrm{E}^{i+1}[\rho^{\tau}]$
11. Computed $\hat{\mathbf{z}}_{k|k}^{\tau}$,$\mathbf{P}_{k|k}^{zz,\tau(i+1)}$ and $\mathbf{P}_{k|k}^{xz,\tau}$ by (41), (42) and (43)
12. $\mathbf{K}_k^{\tau(i+1)} = \mathbf{P}_{k|k}^{xz,\tau}(\mathbf{P}_{k|k}^{zz,\tau(i+1)})^{-1}$
13. $\hat{\mathbf{x}}_{k|k}^{\tau(i+1)} = \hat{\mathbf{x}}_{k|k}^{\tau-1} + \mathbf{K}_k^{\tau(i+1)}(\mathbf{z}_k - \hat{\mathbf{z}}_{k|k}^{\tau})$
14. $\mathbf{P}_{k|k}^{\tau(i+1)} = \mathbf{P}_{k|k}^{\tau-1} - \mathbf{K}_k^{\tau(i+1)}\mathbf{P}_{k|k}^{zz,\tau(i+1)}(\mathbf{K}_k^{\tau(i+1)})^{T}$
end while
15. $\hat{\mathbf{x}}_{k|k}^{\tau} = \hat{\mathbf{x}}_{k|k}^{\tau(\mathrm{M})}, \quad \mathbf{P}_{k|k}^{\tau} = \mathbf{P}_{k|k}^{\tau(\mathrm{M})}$
16. **if** $\eta_\tau < \varepsilon$
break
end for
17. Assimilate the remaining progressive quantity at the ultimate recursion
18. Update $\hat{\mathbf{x}}_{k|k}^{\tau}$, $\mathbf{P}_{k|k}^{\tau}$
19. $\hat{\mathbf{x}}_{k|k} = \hat{\mathbf{x}}_{k|k}^{\tau}, \quad \mathbf{P}_{k|k} = \mathbf{P}_{k|k}^{\tau}$
Outputs: $\hat{\mathbf{x}}_{k|k}$, $\mathbf{P}_{k|k}$, $\alpha_{k,j}$, $\beta_{k,j}$ $(j = 1 \dots m)$

the process noise covariance matrix may be enlarged due to the use of low-cost inertial sensors and the increases of the output errors of gyros. Consequently, the one-step prediction error covariance matrix is also enlarged, which raises the prior uncertainty. During the violent manoeuvering, the output errors of gyros will increase with the same scale factor errors but large angular rate, and then, the process noise covariance matrix and the one-step prediction error covariance matrix are enlarged correspondingly, which will contribute to the prior uncertainty [23]–[37].

B. Nonlinear Measurement Model

Nonlinear measurement models are formed because of the direct use of the raw pseudorange and pseudorange rate in tightly coupled integration systems. Although the EKF can be directly used to carry out the tightly coupled GNSS/INS integration by linearizing the nonlinear integration model based on the first-order Taylor expansion, it suffers from substantial approximation errors for the case of highly nonlinearity. Therefore, on the purpose of improving the approximate accuracy, the nonlinear measurement models with respect to pseudorange and pseudorange rate are established in this article, where the raw pseudorange and pseudorange rate are chosen as the measurements. The nonlinear measurement models can be briefly formulated as follows:

$$\begin{aligned}\rho_s^j &= \sqrt{\left(x-\mathrm{X}_s^j\right)^2+\left(y-\mathrm{Y}_s^j\right)^2+\left(z-\mathrm{Z}_s^j\right)^2}+\delta t_B+\breve{\nu}_{\rho_s^j}\\ &= d^j+\delta t_B+\breve{\nu}_{\rho_s^j} \qquad (56)\\ \dot{\rho}_s^j &= u_x^j\left(v_x-\mathrm{V}_x^j\right)+u_y^j\left(v_y-\mathrm{V}_y^j\right)+u_z^j\left(v_z-\mathrm{V}_z^j\right)+\delta t_D+\breve{\nu}_{\dot{\rho}_s^j} \qquad (57)\end{aligned}$$

where ρ_s^j and $\dot{\rho}_s^j$ denote the measured pseudorange between the receiver and the jth visible satellite as well as the corresponding pseudorange rate, respectively. $(\mathrm{X}_s^j, \mathrm{Y}_s^j, \mathrm{Z}_s^j)$ and $(\mathrm{V}_x^j, \mathrm{V}_y^j, \mathrm{V}_z^j)$ denote the position and surround velocity of the jth visible satellite expressed in e-frame, which can be directly obtained from the Almanac Data. (x, y, z) and (v_x, v_y, v_z) denote the real but unknown position and velocity of the receiver expressed in e-frame. d^j denotes the real but unknown pseudorange. $\breve{\nu}_{\rho_s^j}$ and $\breve{\nu}_{\dot{\rho}_s^j}$ denote the pseudo measurement noises, which are comprehensively induced by the integral approximation errors, the moderately time-varying measurement noises and other non-modeling errors. The pseudo measurement noises are modeled as zero mean Gaussian white noises with nominal MNCM $\bar{\mathbf{R}}_0$. $[u_x^j, u_y^j, u_z^j]^T$ denotes the line of sight vector, which can be given by

$$\left[u_x^j, u_y^j, u_z^j\right]^T=\left[\frac{x-\mathrm{X}_s^j}{d^j}, \frac{y-\mathrm{Y}_s^j}{d^j}, \frac{z-\mathrm{Z}_s^j}{d^j}\right]^T. \qquad (58)$$

Substituting the real but unknown position in (56) and velocity in (57) with the INS providing position (x_{INS}, y_{INS}, and z_{INS}) and velocity ($v_{eb,x}^{e,\mathrm{INS}}$, $v_{eb,y}^{e,\mathrm{INS}}$, and $v_{eb,z}^{e,\mathrm{INS}}$), which are presented in e-frame, respectively, the predicted pseudorange and pseudorange rate can be formulated as follows:

$$\begin{aligned}\hat{\rho}_s^j &= \sqrt{\left(x_{\mathrm{INS}}-\mathrm{X}_s^j\right)^2+\left(y_{\mathrm{INS}}-\mathrm{Y}_s^j\right)^2+\left(z_{\mathrm{INS}}-\mathrm{Z}_s^j\right)^2}+\delta t_B\\ &= d_{\mathrm{INS}}^j+\delta t_B \qquad (59)\\ \hat{\dot{\rho}}_s^j &= u_{x,\mathrm{INS}}^j\left(v_{eb,x}^{e,\mathrm{INS}}-\mathrm{V}_x^j\right)+u_{y,\mathrm{INS}}^j\left(v_{eb,y}^{e,\mathrm{INS}}-\mathrm{V}_y^j\right)\\ &\quad +u_{z,\mathrm{INS}}^j\left(v_{eb,z}^{e,\mathrm{INS}}-\mathrm{V}_z^j\right)+\delta t_D \qquad (60)\end{aligned}$$

where the line of sight vector can be rewritten as

$$\left[u_{x,\mathrm{INS}}^j, u_{y,\mathrm{INS}}^j, u_{z,\mathrm{INS}}^j\right]^T=\left[\frac{x_{\mathrm{INS}}-\mathrm{X}_s^j}{d_{\mathrm{INS}}^j}, \frac{y_{\mathrm{INS}}-\mathrm{Y}_s^j}{d_{\mathrm{INS}}^j}, \frac{z_{\mathrm{INS}}-\mathrm{Z}_s^j}{d_{\mathrm{INS}}^j}\right]^T. \qquad (61)$$

Moreover, the INS providing position solution of receiver presented in e-frame and n-frame conforms the following transformation expression:

$$\begin{bmatrix}x_{\mathrm{INS}}\\ y_{\mathrm{INS}}\\ z_{\mathrm{INS}}\end{bmatrix}=\begin{bmatrix}(\mathrm{R}_N+(\hat{h}_b-\delta h_b))\cos(\hat{L}_b-\delta L_b)\cos(\hat{\rho}_b-\delta\rho_b)\\ (\mathrm{R}_N+(\hat{h}_b-\delta h_b))\cos(\hat{L}_b-\delta L_b)\sin(\hat{\rho}_b-\delta\rho_b)\\ ((\mathrm{R}_N(1-\mathrm{e}^2))+(\hat{h}_b-\delta h_b))\sin(\hat{L}_b-\delta L_b)\end{bmatrix} \qquad (62)$$

where e is the WGS84 eccentricity constant.

The INS providing velocity solution of receiver presented in e-frame and n-frame conforms the following transformation expression:

$$\begin{bmatrix}v_{eb,x}^{e,\mathrm{INS}}\\ v_{eb,y}^{e,\mathrm{INS}}\\ v_{eb,z}^{e,\mathrm{INS}}\end{bmatrix}=\begin{bmatrix}\tau_{11}&\tau_{12}&\tau_{13}\\ \tau_{21}&\tau_{22}&\tau_{23}\\ \tau_{31}&\tau_{32}&\tau_{33}\end{bmatrix}\begin{bmatrix}v_{eb,E}^n-\delta v_{eb,E}^n\\ v_{eb,N}^n-\delta v_{eb,N}^n\\ v_{eb,D}^n-\delta v_{eb,D}^n\end{bmatrix} \qquad (63)$$

where

$$\begin{aligned}\tau_{11} &= -(\mathrm{R}_N+(\hat{h}_b-\delta h_b))\cos(\hat{L}_b-\delta L_b)\sin(\hat{\rho}_b-\delta\rho_b)\\ \tau_{12} &= -(\mathrm{R}_N+(\hat{h}_b-\delta h_b))\sin(\hat{L}_b-\delta L_b)\cos(\hat{\rho}_b-\delta\rho_b)\\ \tau_{13} &= -\cos(\hat{L}_b-\delta L_b)\cos(\hat{\rho}_b-\delta\rho_b)\\ \tau_{21} &= (\mathrm{R}_N+(\hat{h}_b-\delta h_b))\cos(\hat{L}_b-\delta L_b)\cos(\hat{\rho}_b-\delta\rho_b)\\ \tau_{22} &= -(\mathrm{R}_N+(\hat{h}_b-\delta h_b))\sin(\hat{L}_b-\delta L_b)\sin(\hat{\rho}_b-\delta\rho_b)\\ \tau_{23} &= -\cos(\hat{L}_b-\delta L_b)\sin(\hat{\rho}_b-\delta\rho_b)\\ \tau_{31} &= 0\\ \tau_{32} &= (\mathrm{R}_N(1-\mathrm{e}^2)+(\hat{h}_b-\delta h_b))\cos(\hat{L}_b-\delta L_b)\\ \tau_{33} &= -\sin(\hat{L}_b-\delta L_b). \qquad (64)\end{aligned}$$

C. Simulation Analyses

In this simulation, the existing GAFs, the iterated GAFs, and state-of-the-art PGAF are taken into comparison. The EKF [13] and standard CKF [15] are two of the most typical GAFs. The former addresses the nonlinear filtering problem based on the first-order Taylor approximation and the latter addresses this problem based on the sigma-point method. Unfortunately, the EKF often diverges due to large approximation errors that are induced by the large prior uncertainty but high measurement accuracy situation; thus, the simulation results of the EKF are not given in this case. IEKF [29] and IPLF [22] are chosen as the benchmark of other iterated filter algorithms due to their ease of implementation and outstanding performance. Apart from that, the existing PGAF [33] are taken into comparison to verify the superiority of the proposed PGAF with variable step sizes (VS-PGAF). All the filters are configured with identical parameters, such as initial state, initial covariance, system noise covariance matrix, and nominal MNCM. Specially, to balance the estimate accuracy and computational cost, the progressive times of IEKF, IPLF, and the existing PGAF are set as $N = 20$. For VS-PGAF, the discount factor $\varrho = 1 - \exp(-4)$, and $\alpha_{0,j} = 0$ and $\beta_{0,j} = 1$ with $j = 1 \ldots m$.

Case 1 (Situation With Large Prior Uncertainty but High Measurement Accuracy): In this case, to simulate the situation

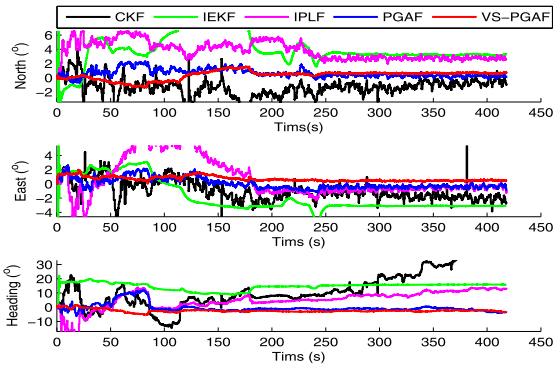

Fig. 2. Attitude errors of the proposed filter and existing filters.

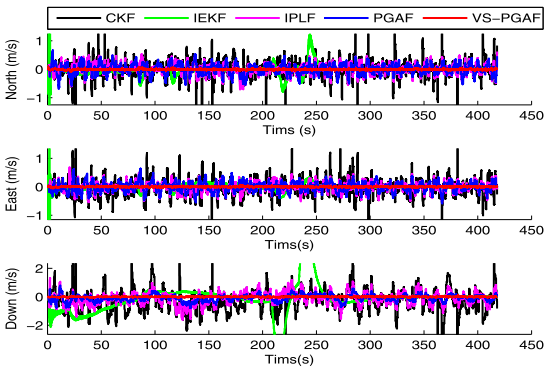

Fig. 3. Velocity errors of the proposed filter and existing filters.

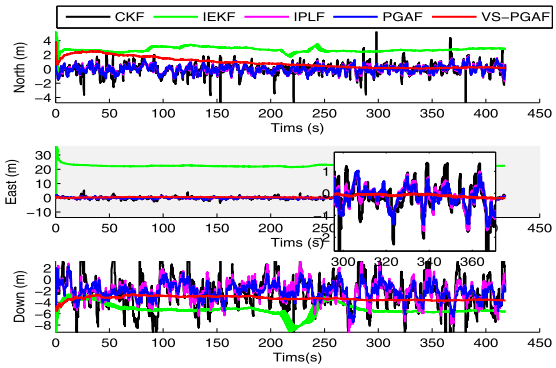

Fig. 4. Position errors of the proposed filter and existing filters.

with large prior uncertainty, violent maneuvering is performed by an aircraft and low-cost consumption grade inertial measurement unit (IMU) is employed. The aircraft maneuvers with two 45° swerve first and then climbs up 500 m at a speed of 200 m/s ending up with level flight. The initial attitude error for pith, roll, and yaw is set as $[-0.5°, 0.4°, 1°]$. The initial bias uncertainty of accelerometers and gyros is set as 10 mg and $200°/\sqrt{\text{h}}$, respectively, and the random noises of accelerometers and gyros are set as 1 $\text{mg}/\sqrt{\text{Hz}}$ and $1°/\sqrt{\text{h}}$, respectively. The bias random walk of accelerometers is set as $0.0032\ \text{m/s}^2/\sqrt{\text{s}}$, and the bias random walk of gyros is set as $0.000362°/\ \text{s}/\sqrt{\text{s}}$. The data output frequency of GNSS and INS are 2 and 100 Hz, respectively. To guarantee the high-accuracy measurements of pseudorange and pseudorange rate, eight satellites are observed. The receiver clock offset and the receiver clock drift at the initial time are set as 10 000 m and 100 m/s. The receiver clock frequency drift and phase drift are set as 1 $\text{m/s}/\sqrt{\text{s}}$ and 1 $\text{m}/\sqrt{\text{s}}$, respectively. The nominal measurement noises standard deviations (SDs) of pseudorange and pseudorange rate are set as 25 m and 1 m/s, which provide the nominal MNCM. The other related satellites' parameters are given in the following. The number of satellites in constellation is 30 and the orbital radius is 26561.75 km. The inclination angle of satellites is 55° and the mask angle is 10°. The residual error SDs for ionosphere and troposphere are set as 2 and 0.2 m, respectively. The code tracking error SD is 1 m, and the range rate tracking error SD is 0.02 m/s. The time duration of the trajectory is 418 s. Furthermore, a closed-loop structure is employed in this system.

The attitude error results estimated by the proposed filter and existing filters are shown in Fig. 2. It is clear to see that the proposed VS-PGAF outperforms the existing filters not only in estimation accuracy but also in the rate of convergence. As shown in Fig. 2, the performance of the standard CKF degrades dramatically because of the situation deteriorated by the large prior uncertainty but high measurement accuracy. This phenomenon is especially obvious in the heading direction. The IEKF and IPLF present some resistance against this situation due to their iterated style, and the IPLF wins the IEKF narrowly on the steady-state performance benefiting from the SLR method it adopted, whereas the existing PGAF is prone to present a better estimate performance, which assimilates the measurement information gradually and makes a sufficient use of that. However, the existing PGAF performs worse than the proposed VS-PGAF both in the estimate accuracy and the rate of convergence limited by the strong dependence on the optimal step sizes choosing. An invariant constant step size may be incompetent in different situations. The adaptively tuned step sizes and more accurate MNCM make the proposed VS-PGAF more splendid.

The north, east, and down velocity errors are shown in Fig. 3. Obviously, the proposed VS-PGAF presents better performances than other filters. The standard CKF performs worst in this situation, followed by IEKF, which presents some unstable fluctuations due to the accumulated Taylor approximation errors during the iterated process. The existing PGAF wins the IPLF narrowly benefiting from the gradual introduction of the measurement information. Both of them are implemented by the sigma-point-based method, which always presents better accuracy than the Taylor approximate method. However, the existing PGAF does not prevail in the proposed VS-PGAF due to the invariant and sub-optimal constant step size.

The north, east, and down position errors are given in Fig. 4. In the north direction, the estimated error of the proposed VS-PGAF is gradually decreased and tends to zero over time. In the east and down directions, the proposed VS-PGAF outperforms other filters obviously. The performance of the standard CKF is degenerated significantly in this situation. The existing PGAF performs slightly better than the IPLF.

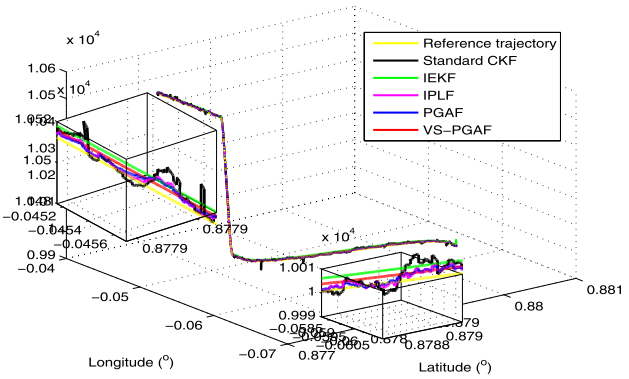

Fig. 5. Real reference trajectory and the trajectories estimated by the proposed filter and existing filters.

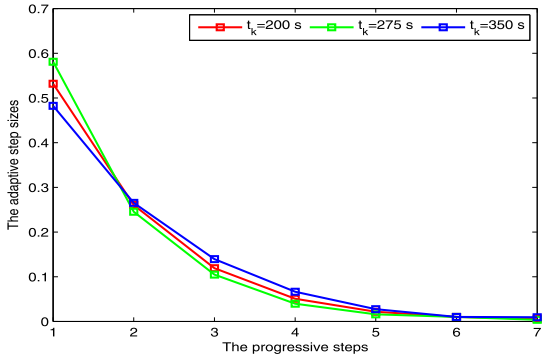

Fig. 6. Adaptively adjusted progressive step sizes at three instants in the proposed filter.

However, due to the poor velocity performance and the accumulated Taylor approximation errors during the iterated process, the IEKF presents larger position estimation biases. The real reference trajectory and the trajectories estimated by different filters are compared in Fig. 5. It is notable that the trajectory estimated by the proposed VS-PGAF approaches the reference more closely than the other trajectories, which reflects a much higher position accuracy than the existing PGAF, the IPLF, the IEKF, and the standard CKF. As shown in Fig. 5, the position accuracy of the existing PGAF is worse than the proposed VS-PGAF but much better than the standard CKF. The IEKF presents larger estimation biases and the IPLF follows the existing PGAF very closely.

Fig. 6 shows the adaptively adjusted progressive step sizes at different and random instants in the proposed filter. The result reveals that much fewer progressive steps are needed in the proposed VS-PGAF in spite of much higher estimation accuracy that is presented compared with the existing PGAF, the IEKF, as well as the IPLF, where the iteration times are set as $N = 20$. The optimal step sizes of the proposed VS-PGAF are inferred online based on the VB approach.

In order to verify the superiority of the proposed VS-PGAF statistically, the Monte Carlo (MC) runs are adopted. The root mean square error (RMSE) is taken to evaluate the estimation accuracy of different filters and the SD, which is the square root of variance (VAR), is taken to evaluate the steady-state fluctuations. The RMSE is defined as follows:

$$\mathrm{RMSE}_a = \sqrt{\frac{1}{MT}\sum_{k=1}^{T}\sum_{s=1}^{M}\left(x_{a,k}^{s} - \hat{x}_{a,k}^{s}\right)^2} \tag{65}$$

and the VAR is defined as follows:

$$\mathrm{VAR}_a = \frac{1}{MT}\sum_{k=1}^{T}\sum_{s=1}^{M}\left(\hat{x}_{a,k}^{s} - \mathrm{RMSE}_a\right)^2 \tag{66}$$

where M denotes the number of MC run and T denotes the simulation time. $x_{a,k}^{s}$ and $\hat{x}_{a,k}^{s}$ denote the true and estimated state variable at the sth MC run and the kth time instant, respectively. Subscript a can be substituted by arbitrary name of element, such as Yaw, Pitch, Poll, VN, VE, and VD (velocity on the north, east, and down direction), PN, PE, and PD (position on the north, east, and down direction). Furthermore, the RMSE of position ($\mathrm{RMSE}_{\mathrm{pos}}$) can be calculated by

$$\mathrm{RMSE}_{\mathrm{pos}} = \mathrm{RMSE}_{PN} + \mathrm{RMSE}_{PE} + \mathrm{RMSE}_{PD} \tag{67}$$

and the SD of position ($\mathrm{SD}_{\mathrm{pos}}$) can be calculated by

$$\mathrm{SD}_{\mathrm{pos}} = \sqrt{\mathrm{VAR}_{PN} + \mathrm{VAR}_{PE} + \mathrm{VAR}_{PD}} \tag{68}$$

and the RMSE of velocity ($\mathrm{RMSE}_{\mathrm{vel}}$) and the RMSE of attitude ($\mathrm{RMSE}_{\mathrm{att}}$) as well as the SD of velocity ($\mathrm{SD}_{\mathrm{vel}}$) and the SD of attitude ($\mathrm{SD}_{\mathrm{att}}$) can be obtained by the similar method. By setting $M = 50$, $\mathrm{RMSE}_{\mathrm{pos}}$, $\mathrm{RMSE}_{\mathrm{vel}}$, and $\mathrm{RMSE}_{\mathrm{att}}$ as well as $\mathrm{SD}_{\mathrm{pos}}$, $\mathrm{SD}_{\mathrm{vel}}$, and $\mathrm{SD}_{\mathrm{att}}$ over the last 100 s are listed in Table II. Table II reveals that in the statistical sense, the proposed VS-PGAF presents much higher estimation accuracy but much smaller steady fluctuation in position, velocity, and attitude than other filters. In terms of position, although the IEKF performs quite smoothly, large biases are induced due to the strong nonlinearity of the measurement model and the accumulated Taylor approximation errors. The standard CKF presents severe fluctuations and very high estimation errors in the situation with large prior uncertainty but high measurement accuracy. The proposed VS-PGAF has been improved by 16.84%, 91.98%, and 73.93% on estimation accuracy and has been decreased by 93.32%, 91.60%, and 83.02% on steady fluctuation over the IPLF in position, velocity, and attitude, respectively, and the proposed VS-PGAF has been improved by 4.26% and 89.23% on estimation accuracy and has been decreased by 92.03% and 88.40% on steady fluctuation over the existing PGAF in position and velocity, respectively. The simulations are coded with MATLAB and run on a computer with Intel Core i5-3470 CPU at 3.20 GHz. The implementation times of the proposed filter and existing filters are listed in Table III. It can be seen from Table III that the implementation time of the proposed VS-PGAF is greater than the existing filters, but the estimation accuracy has been significantly improved over the existing filters.

Case 2 (Regular Situation): In this case, a higher precision IMU is employed and natural maneuvering is carried out by the vehicle to simulate the regular situation. The vehicle maneuvers at a speed of 20 m/s and two opposite direction 45° swerve are performed during the maneuvering. The initial attitude error for pith, roll, and yaw is set as

TABLE II

STATISTICAL PERFORMANCE COMPARISON OVER THE LAST 100 s (RMSE±SD)

Filters	Position(m)	Velocity(m/s)	Attitude(°)
Standard CKF	4.788±2.901	1.221±0.904	33.650±9.732
IEKF	30.784±0.181	0.104±0.075	22.165±0.101
IPLF	3.926±1.707	0.561±0.250	13.926±2.032
Existing PGAF	3.401±1.430	0.418±0.181	2.251±1.022
VS-PGAF	3.265±0.114	0.045±0.021	3.630±0.345

TABLE III

IMPLEMENTATION TIMES OF THE PROPOSED FILTER AND EXISTING FILTERS

Filters	CKF	IEKF	IPLF	PGAF	VS-PGAF
Time(s)	72.72	52.80	508.63	505.83	1007.4

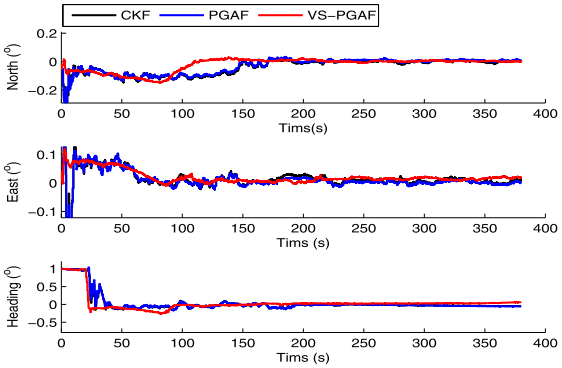

Fig. 7. Attitude errors of the proposed filter and existing filters.

$[-0.05°, 0.04°, 1°]$. The initial bias uncertainty of accelerometers and gyros is set as 1 mg and $10°/\sqrt{\text{h}}$, respectively, and the random noises of accelerometers and gyros are set as 0.1 mg/$\sqrt{\text{Hz}}$ and $0.01°/\sqrt{\text{h}}$, respectively. The bias random walk of accelerometers is set as 0.00032 m/s^2/$\sqrt{\text{s}}$, and the bias random walk of gyros is set as 0.000081°/ s/$\sqrt{\text{s}}$. The data output frequency of GNSS and INS is 2 and 100 Hz, respectively. In this simulation, eight satellites are observed. The receiver clock offset and the receiver clock drift at the initial time are set as 10 000 m and 100 m/s. The receiver clock frequency drift and phase drift are set as 1 m/s/$\sqrt{\text{s}}$ and 1 m/$\sqrt{\text{s}}$, respectively. The measurement noises' SDs of pseudorange and pseudorange rate are set as 50 m and 2 m/s, respectively. The other related satellites parameters are the same as Case 1. The time duration of trajectory is 380 s. Furthermore, a closed-loop structure is employed in this system. In this case, the standard CKF, the existing PGAF, and the proposed VS-PGAF are taken into comparison. All the filters are configured with identical parameters, such as initial state, initial covariance, system noise covariance matrix, and MNCM. The progressive time of the existing PGAF is set as $N = 20$.

The attitude, velocity, and position errors estimated by the proposed filter and the existing filters are shown in Figs. 7–9. It is clearly to learn from Fig. 7 that in terms of attitude, the proposed VS-PGAF outperforms the existing filters not only in estimate accuracy but also in the rate

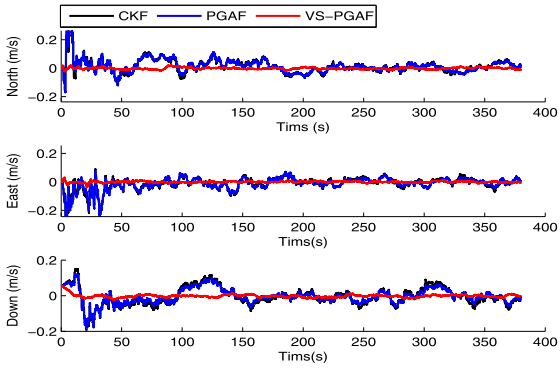

Fig. 8. Velocity errors of the proposed filter and existing filters.

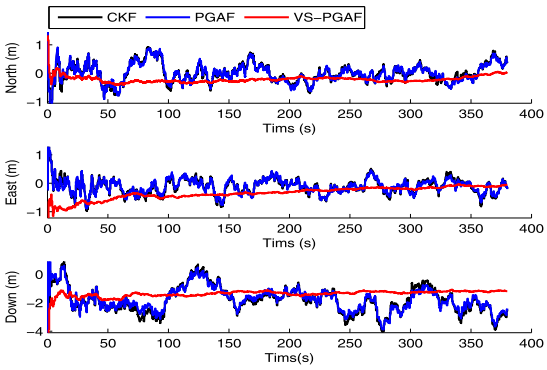

Fig. 9. Position errors of the proposed filter and existing filters.

TABLE IV

STATISTICAL PERFORMANCE COMPARISON OVER THE LAST 100 s (RMSE±SD)

Filters	Position(m)	Velocity(m/s)	Attitude(min)
Standard CKF	2.293±0.811	0.0754±0.032	2.982±0.011
Existing PGAF	2.321±0.641	0.0582±0.025	3.30±0.011
VS-PGAF	1.544±0.114	0.0132±0.005	3.258±0.007

of convergence. It can also be seen from Fig. 8 that the proposed VS-PGAF presents higher estimation accuracy and more excellent steady-state performance than the CKF and existing PGAF in velocity. As for the position, the estimated errors of the proposed VS-PGAF is gradually convergent and tends to zero over time, while the CKF and the existing PGAF are fluctuating around the zero line. The CKF and the existing PGAF have a similar performance in terms of attitude, velocity, and position because the existing PGAFs are degenerated into the standard CKF in the regular situation.

In order to analyze the simulation results statistically, the MC runs are adopted. The RMSE and SD, calculated as (65)–(68), are taken to evaluate the estimation accuracy and the steady-state fluctuations, respectively. By setting $M = 50$, RMSE_{pos}, RMSE_{vel}, and RMSE_{att} as well as SD_{pos}, SD_{vel}, and SD_{att} over the last 100 s are listed in Table IV. Table IV reveals that in the regular situation, the proposed VS-PGAF presents much higher estimation accuracy but much smaller steady fluctuation in position and velocity. In attitude, the RMSE of the proposed VS-PGAF is a little inferior to the

CKF, but it performs more smoothly than the existing filters. In summary, the proposed VS-PGAF performs well even in the regular situation, which is due to the adaptive and real-time modification of the inaccurate MNCM.

V. Conclusion

In this article, a novel PGAF with variable step size and adaptive MNCM (VS-PGAF) was developed to improve the estimation accuracy in the situation with large prior uncertainty but high measurement accuracy. The state vector, the step sizes, as well as the inaccurate MNCM are jointly estimated based on the VB method in the proposed algorithm. Compared with the existing PGAF, the proposed filter can achieve better estimation accuracy, but significantly fewer progressive steps are required. Simulation results of tightly coupled GNSS/INS integration illustrated that the proposed filter outperforms the existing filters both in estimation accuracy and rate of convergence. The proposed filter focuses on addressing the nonlinear filtering problem with Gaussian process and measurement noises. However, the proposed filter may be unsuitable when the measurement noise has a non-Gaussian distribution.

Acknowledgment

The authors thank to the suggestions from the Associate Editor and the reviewers, which really help to improve the quality of this paper. The authors are grateful to Dr. Paul Groves, who is the author of [25], and the implemented codes are based on his open source works. The codes and data of this paper have been archived on https://www.researchgate.net/profile/Yulong_Huang3.

References

[1] H. Qi and J. B. Moore, "Direct Kalman filtering approach for GPS/INS integration," *IEEE Trans. Aerosp. Electron. Syst.*, vol. 38, no. 2, pp. 687–693, Apr. 2002.

[2] Q. Xu, X. Li, and C.-Y. Chan, "Enhancing localization accuracy of MEMS-INS/GPS/in-vehicle sensors integration during GPS outages," *IEEE Trans. Instrum. Meas.*, vol. 67, no. 8, pp. 1966–1978, Aug. 2018.

[3] Y. Huang, Y. Zhang, and X. Wang, "Kalman-filtering-based in-motion coarse alignment for odometer-aided SINS," *IEEE Trans. Instrum. Meas.*, vol. 66, no. 12, pp. 3364–3377, Dec. 2017.

[4] J. L. Crassidis, "Sigma-point Kalman filtering for integrated GPS and inertial navigation," *IEEE Trans. Aerosp. Electron. Syst.*, vol. 42, no. 2, pp. 750–756, Apr. 2006.

[5] D. A. Grejner-Brzezinska, C. K. Toth, H. Sun, X. Wang, and C. Rizos, "A robust solution to high-accuracy geolocation: Quadruple integration of GPS, IMU, pseudolite, and terrestrial laser scanning," *IEEE Trans. Instrum. Meas.*, vol. 60, no. 11, pp. 3694–3708, Nov. 2011.

[6] C. K. Toth, "Sensor integration in airborne mapping," *IEEE Trans. Instrum. Meas.*, vol. 51, no. 6, pp. 1367–1373, Dec. 2002.

[7] J. F. Wagner and G. Kasties, "Applying the principle of integrated navigation systems to estimating the motion of large vehicles," *Aerosp. Sci. Technol.*, vol. 8, no. 2, pp. 155–166, Mar. 2004.

[8] Y. Li, J. Wang, C. Rizos, P. Mumford, and W. Ding, "Low-cost tightly coupled GPS/INS integration based on a nonlinear Kalman filtering design," in *Proc. ION Nat. Tech. Meeting*, Jan. 2006, pp. 18–20.

[9] G. Hu, S. Gao, and Y. Zhong, "A derivative UKF for tightly coupled INS/GPS integrated navigation," *ISA Trans.*, vol. 56, pp. 135–144, May 2015.

[10] A. Sharma, S. C. Srivastava, and S. Chakrabarti, "A cubature Kalman filter based power system dynamic state estimator," *IEEE Trans. Instrum. Meas.*, vol. 66, no. 8, pp. 2036–2045, Aug. 2017.

[11] K. Ito and K. Xiong, "Gaussian filters for nonlinear filtering problems," *IEEE Trans. Autom. Control*, vol. 45, no. 5, pp. 910–927, May 2000.

[12] Y. L. Huang, Y. Zhang, X. Wang, and L. Zhao, "Gaussian filter for nonlinear systems with correlated noises at the same epoch," *Automatica*, vol. 60, pp. 122–126, Oct. 2015.

[13] B. D. O. Anderson and J. B. Moore, *Optimal Filtering*. Englewood Cliffs, NJ, USA: Prentice-Hall, 1979, pp. 105–106.

[14] S. J. Julier and J. K. Uhlmann, "Unscented filtering and nonlinear estimation," *Proc. IEEE*, vol. 92, no. 3, pp. 401–422, Mar. 2004.

[15] I. Arasaratnam and S. Haykin, "Cubature Kalman filter," *IEEE Trans. Autom. Control*, vol. 54, no. 6, pp. 1254–1269, May 2009.

[16] B. Jia, M. Xin, and Y. Cheng, "High-degree cubature Kalman filter," *Automatica*, vol. 49, no. 2, pp. 510–518, Feb. 2013.

[17] Y. Zhang, Y. Huang, N. Li, and L. Zhao, "Embedded cubature Kalman filter with adaptive setting of free parameter," *Signal Process.*, vol. 114, no. 3, pp. 112–116, Sep. 2015.

[18] Y. Zhang, Y. Huang, N. Li, and L. Zhao, "Interpolatory cubature Kalman filters," *IET Control Theory Appl.*, vol. 9, no. 11, pp. 1731–1739, Jul. 2015.

[19] B. Jia, M. Xin, and Y. Cheng, "Sparse-grid quadrature nonlinear filtering," *Automatica*, vol. 48, no. 2, pp. 327–341, 2012.

[20] J. Duník, O. Straka and M. Šimandl, "Stochastic integration filter," *IEEE Trans. Autom. Control*, vol. 58, no. 6, pp. 1561–1566, Jun. 2013.

[21] M. R. Morelande and Á. F. García-Fernández, "Analysis of Kalman filter approximations for nonlinear measurements," *IEEE Trans. Signal Process.*, vol. 61, no. 22, pp. 5477–5484, Nov. 2013.

[22] Á. F. García-Fernández, L. Svensson, M. R. Morelande, and S. Särkkä, "Posterior linearization filter: Principles and implementation using sigma points," *IEEE Trans. Signal Process.*, vol. 63, no. 20, pp. 5561–5573, Oct. 2015.

[23] L. Chang, K. Li, and B. Hu, "Huber's M-estimation-based process uncertainty robust filter for integrated INS/GPS," *IEEE Sensors J.*, vol. 15, no. 6, pp. 3367–3374, Jun. 2015.

[24] Y. Huang and Y. Zhang, "A new process uncertainty robust student's t based Kalman filter for SINS/GPS integration," *IEEE Access*, vol. 5, pp. 14391–14404, 2017.

[25] P. D. Groves, *Principles of GNSS, Intertial, and Multisensory Integrated Navigation Systems*, 3rd ed. Boston, MA, USA: Artech House, 2013, pp. 584–606.

[26] Y. Stebler, S. Guerrier, and J. Skaloud, "An approach for observing and modeling errors in MEMS-based inertial sensors under vehicle dynamic," *IEEE Trans. Instrum. Meas.*, vol. 64, no. 11, pp. 2926–2936, Nov. 2015.

[27] M. S. Arulampalam, S. Maskell, N. Gordon, and T. Clapp, "A tutorial on particle filters for online nonlinear/non-Gaussian Bayesian tracking," *IEEE Trans. Signal Process.*, vol. 50, no. 2, pp. 174–188, Feb. 2002.

[28] L. Mihaylova, A. Y. Carmi, F. Septier, A. Gning, S. K. Pang, and S. Godsill, "Overview of Bayesian sequential Monte Carlo methods for group and extended object tracking," *Digit. Signal Process.*, vol. 25, pp. 1–16, Feb. 2014.

[29] B. M. Bell and F. W. Cathey, "The iterated Kalman filter update as a Gauss-Newton method," *IEEE Trans. Autom. Control*, vol. 38, no. 2, pp. 294–297, Feb. 1993.

[30] U. D. Hanebeck, "PGF 42: Progressive Gaussian filtering with a twist," in *Proc. 16th Int. Conf. Inf. Fusion*, Istanbul, Turkey, Jul. 2013, pp. 1103–1110.

[31] J. Steinbring and U. Hanebeck, "Progressive Gaussian filtering using explicit likelihoods," in *Proc. 17th Int. Conf. Inf. Fusion (Fusion)*, Salamanca, Spain, Jul. 2014, pp. 1–8.

[32] R. Zanetti, "Recursive update filtering for nonlinear estimation," *IEEE Trans. Autom. Control*, vol. 57, no. 6, pp. 1481–1490, Jun. 2012.

[33] Y. Huang, Y. Zhang, N. Li, and L. Zhao, "Gaussian approximate filter with progressive measurement update," in *Proc. IEEE 54th Annu. Conf. Decis. Control (CDC)*, Osaka, Japan, Dec. 2015, pp. 4344–4349.

[34] Á. F. García-Fernández and L. Svensson, "Gaussian MAP filtering using Kalman optimization," *IEEE Trans. Autom. Control*, vol. 60, no. 5, pp. 1336–1349, May 2015.

[35] N. Oudjane and C. Musso, "Progressive correction for regularized particle filters," in *Proc. 3rd Int. Conf. Inf. Fusion*, Paris, France, vol. 2, Jul. 2000, pp. THB2/10–THB2/17.

[36] M. Fatemi, L. Svensson, L. Hammarstrand, and M. Morelande, "A study of MAP estimation techniques for nonlinear filtering," in *Proc. 15th Int. Conf. Inf. Fusion*, Singapore, Jul. 2012, pp. 1058–1065.

[37] M. Y. Zhong, J. Guo, and Q. Cao, "On designing PMI Kalman filter for INS/GPS integrated systems with unknown sensor errors," *IEEE Sensors J.*, vol. 15, no. 1, pp. 535–544, Jan. 2015.

[38] X. Wang, Y. Liang, Q. Pan, and F. Yang, "A Gaussian approximation recursive filter for nonlinear systems with correlated noises," *Automatica*, vol. 48, no. 9, pp. 2290–2297, 2012.
[39] A. O'Hagan and J. J. Forster, *Kendall's Advanced Theory of Statistics: Bayesian Inference*. London, U.K.: Arnold, 2004.
[40] Y. Huang, Y. Zhang, N. Li, and L. Zhao, "Design of sigma-point Kalman filter with recursive updated measurement," *Circuits Syst. Signal Process.*, vol. 35, no. 5, p. 1767–1782, May 2016.
[41] C. M. Bishop, *Pattern Recognition and Machine Learning*. Berlin, Germany: Springer, 2007.
[42] D. G. Tzikas, A. C. Likas, and N. P. Galatsanos, "The variational approximation for Bayesian inference," *IEEE Signal Process. Mag.*, vol. 25, no. 6, pp. 131–146, Jan. 2008.
[43] Y. Huang, Y. Zhang, Z. Wu, N. Li, and J. Chambers, "A novel adaptive Kalman filter with inaccurate process and measurement noise covariance matrices," *IEEE Trans. Autom. Control*, vol. 63, no. 2, pp. 594–601, Feb. 2017.

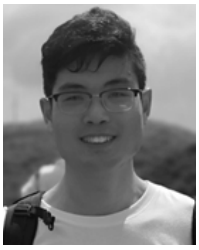

Mingming Bai received the B.S. degree from the Department of Automation, China University of Geosciences, Wuhan, China, in 2016. He is currently pursuing the Ph.D. degree in control science and engineering with Harbin Engineering University, Harbin, China.

His current research interests include signal processing, information fusion, and their applications in navigation technology, such as inertial navigation and integrated navigation.

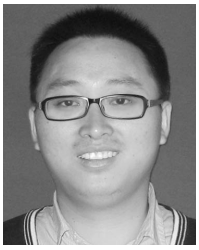

Yulong Huang (M'19) received the B.S. degree in automation and the Ph.D. degree in control science and engineering from the Department of Automation, Harbin Engineering University (HEU), Harbin, China, in 2012 and 2018, respectively.

From November 2016 to November 2017, he was a Visiting Graduate Researcher with the Electrical Engineering Department, Columbia University, New York, NY, USA. He is currently an Associate Professor of navigation, guidance, and control with HEU. His current research interests include signal processing, information fusion, and their applications in navigation technology, such as inertial navigation and integrated navigation.

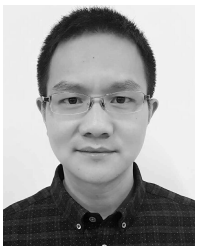

Yonggang Zhang (S'06–M'07–SM'16) received the B.S. and M.S. degrees from the Department of Automation, Harbin Engineering University (HEU), Harbin, China, in 2002 and 2004, respectively, and the Ph.D. degree in electronic engineering from Cardiff University, Cardiff, U.K., in 2007.

He was a Post-Doctoral Fellow with Loughborough University, Loughborough, U.K., from 2007 to 2008, in the area of adaptive signal processing. He is currently a Professor of navigation, guidance, and control with HEU. His current research interests include signal processing, information fusion, and their applications in navigation technology, such as fiber optical gyroscope, inertial navigation, and integrated navigation.

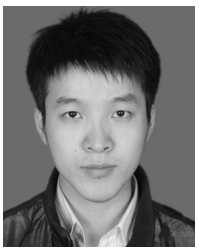

Guangle Jia received the B.S. degree from the School of Safety Engineering, North China Institute of Science and Technology, Langfang, China, in 2013, and the M.S. degree from the Department of Automation, Harbin Engineering University, Harbin, China, in 2017, where he is currently pursuing the Ph.D. degree in control science and engineering.

His current research interests include signal processing, information fusion, and their applications in navigation technology, such as inertial navigation and integrated navigation.